Incorporating polymers to reduce cost of smart windows

A report prepared by Team Smart Cicadas: Jake Steiner, Glenn Pastel, Ryan Tillman, Kari McPartland, Esha Murty, and Soo-Hwan Jang on May 14, 2014 for ENMA490

TABLE OF CONTENTS

Motivation

Increasing pursuit for low environmental impact designs of buildings is spurring development of so-called "smart windows," glass materials capable of changing their optical properties in response to the environment, to minimize energy costs associated with heat lost (or gained) via windows with the outside.[1-4] The most promising type of smart windows for commercialization switches between a transparent and absorbing optical mode through an applied voltage. Materials which undergo this change are termed electrochromic.

Recently, a group led by Kazumi Tajima in Japan has developed a smart window system in which an electrochromic material transforms from transparent to reflective,[2] an optical property which deters radiative heating more so than absorbing materials. Development of such a device could advance the technology beyond recent commercialization of smart windows which only transition between transparent and absorbing states.

Their solid-state device consists of a layered structure of glass/ITO/Mg_4Ni/Pt/PEI/WO_3/ITO/glass, where ITO serves a transparent conducting electrode; Mg_4Ni/Pt absorbs and desorbs hydrogen to transition from transparent to reflecting; PEI serves as a hydrogen electrolyte; and WO_3 takes in hydrogen to be stored when it is not infiltrating the Mg_4Ni.

The use of materials like ITO and WO_3, limit the ultimate commercialization of such a technology due to their high expense. We are proposing a modification to Tajima's group's design which involves replacing these more expensive materials with organic substitutes poly(3,4-ethylenedioxythiophene)-polystyrenesulfonate (PEDOT:PSS) and polyaniline (PANI) in an effort to reduce costs from both production and processing while maintaining the properties of their reflective smart window device.

Previous Work

To obtain variable optical properties, smart windows take advantage of solid-state redox reactions which occur via cation transport—typically H^+ or Li^+—across an electrolyte into a storing material.[1] The cation diffuses into the storing material, most commonly WO_3, and can alter the crystalline structure and local electron density, causing a large change in optical properties. In the case of WO_3, a transparent, ionic material, the intake of H^+ forms H_xWO_3 which absorbs most visible light, and has a deep blue appearance.[1] In order to induce diffusion, an electric potential is applied between two transparent electrodes, so smart windows typically have a layered structures with configuration: glass substrate/transparent electrode/active layer/proton electrolyte/proton storage layer/transparent electrode/glass substrate.

The technology has attracted a substantial amount of research over the past two decades in an attempt to find an optimal materials configuration which would satisfy potential consumer demands. In a review published by Ruben Baetens et al. in 2013,[1] Baetens states a list of specifications necessary in order to make smart windows an attractive prospect for incorporation of sustainable design in buildings. This includes being able to transition between 10-50% transparency under 3 or less volts for small samples, or less than 24 volts for the ultimate goal of smart windows 3 x 2 m^2 in size. In addition, the windows must be operable between -30 and 70^{oC} in anticipation of environmental considerations, and have a lifetime greater than 10^4 cycles.

The most commonly used active layer material in the industry is WO_3 due to satisfying most of these commercial demands, although there are still quite some difficulties faced in manufacturing large enough layers for 3 x 2 m^2 sheets. Similarly, ITO is widely used in the industry in order to apply voltages

over large sheets of glass, due to its superior properties. However, the search for material alternatives to ITO and WO_3 is still ongoing, considering the expense involved in using vapor processing techniques to fabricate large sheets of the materials. Other materials include Nb-, Ni-, and Ir-based oxides, which do little to ease the burden of expense, or polymer-based alternatives, including poly(3,4-ethylene-dioxythiophene) (PEDT) and polyaniline (PANI), which are electrochromic but have not yet seen detailed research into extending product lifetime against ultraviolet degradation.[1]

The advent of reflective smart windows, or switchable mirrors, relies on the use of Mg_xNi reacting with hydrogen cations to transition from reflective amorphous Mg/Mg_2Ni to transparent $MgH_2/MgNiH_4$.[5] Although Mg has seen extensive research for use as a hydrogen storage material, little research has been done on its electrochromic properties. Tajima's group determined in previous work that the optimal stoichiometric configuration for Mg_xNi is Mg_4Ni in terms of performance for a smart window device.[5]

In order to make processing of the Mg_4Ni-based smart windows both cheaper and simpler, Tajima's group incorporated a proton polymer electrolyte, polyethyleneimine (PEI), to serve as an adhesive between their layered structure. Their device had a structure of glass/ITO/Mg_4Ni/PEI/H_xWO_3/ITO/glass. In the transparent state, their device had between 30-43% transmittance over the visible spectrum, and in the reflective state, their device had approximately 50% reflectance over the visible spectrum. The time to transition from reflective to transparent under an applied voltage of 3V was 30s, and the time to transition back under an applied voltage of -3V was 65s.[2]
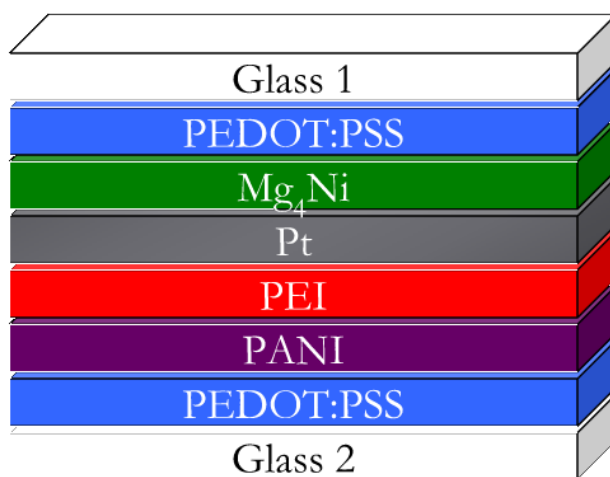

Figure 1 A conceptual diagram of the layered structure we proposed to manufacture. The PEDOT:PSS layers serve as transparent conducting electrodes. Upon application of a voltage, hydrogen will diffuse out of the PANI storage layer, cross through the PEI hydrogen electrolyte, and react with the Mg_4Ni to form $Mg_2H/MgNiH_4$.

Summary of Proposed Work

Materials like ITO and WO_3, though widely developed and commercially available, are expensive enough to warrant a search for alternatives. In an effort to reduce the cost for the development of a similar reflective smart window to that of Tajima's group, we propose creating a layered structure that substitutes organic materials for ITO and WO_3: glass/PEDOT:PSS/Mg_4Ni/Pt/PEI/PANI/PEDOT:PSS/glass. A conceptual diagram of this structure is shown in Figure 1. The goal would be to create a switchable mirror

device with properties that at least rival, if not surpass those of Tajima's group: 30-43% transmittance over the visible spectrum in the transparent state, 50% reflectance over the visible spectrum in the reflective state, a switching time between 30-60s, and powered by 5 or less volts.

Both PEDOT:PSS and PANI are electrochromic materials which have seen study over the past decade, but they have seen less development due to limitations of their properties. PEDOT:PSS, upon oxidation, changes from blue to transparent, and it also conducts electricity well while in this transparent state. However, this polymer has low cycling ability and is susceptible to UV degradation. PANI, upon oxidation, changes from transparent to violet, and has very good cyclability (up to 10^6 cycles). However, its switching speed has shown to be lacking; it can be on the order of tens of minutes, which is much higher than 30-60s for WO_3.

The drawbacks of these polymers, however, manifest when they are used as the active electrochromic layer for smart window devices. With this proposed design, the PEDOT:PSS would instead act as a transparent conducting electrode, and the PANI would instead act as a proton storage layer for when the Mg_4Ni layer is reduced to achieve transparency. Although this does not necessarily solve the problem of UV degradation, in the case of PEDOT:PSS, that is a matter which could be further investigated in future research.

What makes this device structure attractive is the ease with which it may be processed. PEDOT:PSS may be purchased in solution under the brand name Clevios,[6] from which it can be deposited more easily than a sputtered ceramic material. PANI, however, is not commercially available, and it must be doped with hydrogen during processing in order for it to act as a source of hydrogen for device operation. Typically, this is done via chemical synthesis in acidic solution, under which the processing conditions may drastically affect the properties of the PANI layer.[4] The design and refinement of this process will be one major focus of this project.

In addition, we would like to perform electrical and optical analyses in order to inform processing decisions in choosing the shape of the device, the thickness of each separate layer, the doping required, and to predict device properties before testing.

Technical Approach

We present in this section a broad description of the various methods which we looked into and/or employed in completion of our project. This includes our modelling approach for electrical and optical behavior, the processing technique used for each of our layers, and what characterization methods we used. Our initial review of existing literature for important material parameters of each separate layer was lacking in information which would allow us to perform different sets of electrical and optical calculations. We initially thought these calculations would allow us to better plan for design of a layered device. Without them, we shifted to a design approach of prototyping concurrently with modelling/numerical calculations. Because of this shift, we decided to move ahead with processing each material layer based on methods described elsewhere.[2,5-7] After the manufacture of each layer, we performed our own materials' characterization measurements that we had available to us in order to develop models and calculations to ultimately compare with the prototype's performance.

Manufacturing

Device fabrication procedures are summarized in Figure 2. We created the final prototype by depositing thin films through the various methods outlined below in the order shown on the flowchart.

Starting with two separate glass slides, the two halves are then glued together as the thermoset PEI layer cures, which then doubles as an electrolyte for the final device.
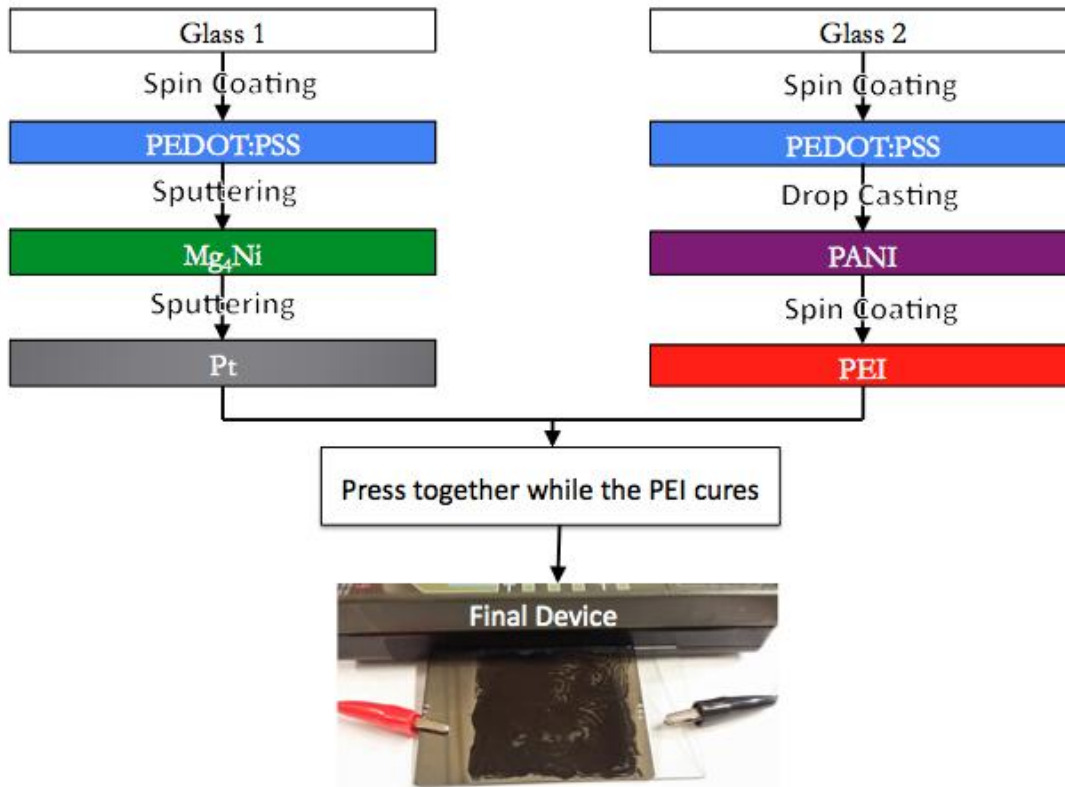

Figure 2: Prototyping flowchart

Polymer Synthesis

PEDOT:PSS

Synthesis of the PEDOT:PSS was one of the more simple procedures of our project. The chemicals used were a 1.1% solution of PEDOT:PSS in water and DMSO (dimethylsulfoxide) which was available for purchase commercially. DMSO is a high boiling point, water-miscible, polar organic solvent, which is important for dispersing the conductive polymer while preserving its conductive properties.[6] In order to achieve a 5% wt DMSO solution, we weighed out 10.09g of 1.1% PEDOT:PSS and added .53g of DMSO, to reach a total solution mass of 10.62g. We proceeded to double the volume of the solution by adding methanol in order to improve the wetting characteristics of the solution onto soda-lime glass, making spin-coating easier and more uniform.

PANI

For the synthesis of PANI, we loosely followed the procedure outlined in an article by Dr. Kaner's group from the University of California, Los Angeles.[7] The chemicals needed for this synthesis were hydrochloric acid, aniline and ammonium peroxydisulfate. First, we diluted the hydrochloric acid to

achieve a solution of 2.6 pH. The accuracy of the pH was vital to achieving dispersion of the nanofibers.[7] We weighed out .036g of ammonium peroxydisulfate and mixed it with 5mL of the diluted acid solution. We made sure it dissolved into a homogeneous solution and then added 60μL of aniline. These result in a 4:1 molar ratio portion which is crucial to the success of the reaction. Then, we added 20mL more of the dilute acid solution so that we would have a ~25mL suspension of PANI. In the method outlined by Dr. Kaner's group from the University of California, Los Angeles it took about 15 hours for the PANI nanofibers to disperse while being heated at ~105∘C. This was not a practical approach for us, as we wouldn't be able to watch over the heating solution for 15 hours. Instead, we left our mixture at room temperature for over 24 hours as we waited for the fibers to disperse. We obtained a solution that looked similar to the figure in Dr. Kaner's paper; it was an opaque dark green solution with small particles of the polymer dispersed evenly throughout.

<u>PEI</u>

PEI is the adhesive solution we used for our prototype. In order to synthesize it, we mixed .5g of polyvinyl butyral with 10mL of gamma-butyralactone while heating the mixture at ~50∘C to aid in dissolution. After the mixture was homogenous and completely dissolved, we added .1mL of polyethyleneimine and continued to heat until completely dissolved. This took about 20 minutes, as the two solutions were of very different viscosities.

Deposition Methods

We tried a variety of different deposition methods in making polymer thin films for our device. These include spin-coating, Meyer Rod, and drop-casting, all of which can be done with relative ease as compared to sputtering.

<u>Spin-coating</u>

We used spin-coating to deposit our film of PEDOT:PSS as well as our adhesive PEI layer. Spin-coating involves pipetting a small amount of solution onto a substrate, then rotating the substrate at high speeds to spread the film out and make it uniform. Because of the difference in viscosities of the different polymers, we used different settings on the spin coater to get a thin, uniform film. For PEDOT:PSS, we set the spin coater at 2000 RPM, ramping it up to that speed in 5 seconds, and held it at that speed for 60 seconds.

<u>Meyer Rod</u>

Towards the middle of the semester, we tried using the Meyer Rod deposition method for PEDOT:PSS in an attempt to wet our glass substrates more evenly. Before we added methanol to our solution, spin coating was not giving us a thin, uniform layer. Instead, the layer was very uneven and unsuitable. A Meyer Rod is a stainless steel rod which is wound tightly with stainless wire of varying diameter. We pipette enough solution to coat the entire slide and then roll the rod over and down the slide, covering it in solution. The thickness of the layer is controlled by the thickness of the wire wrapped around the rod, and this can be chosen by the user. We chose a wire thickness of 1μm. This method, however, did not prove any better than spin-coating and was far more involved, so we abandoned it and decided to keep troubleshooting our spin-coating methods.

Drop Casting

Drop casting was a method we used to deposit PANI when we found that our spin coated layers were too thin. In order to use drop casting, our PANI suspension needed to be concentrated. We centrifuged the solution until we had about 2-3mL of concentrated PANI solution. We set the glass slide on a hot plate at ~60∘C and pipetted the concentrated PANI uniformly across the slide. We waited for about 15 minutes for the solvent to evaporate off, and achieved a somewhat uniform layer of PANI on our slide. We continued using this method for the rest of our PANI depositions and for our final prototype.

Sputtering

To obtain a Mg_4Ni layer with Pt layer atop it with the appropriate stoichiometry and thickness, we decided to utilize the AJA Sputtering Unit in the Maryland Nanocenter to deposit these inorganic films. One requirement of our Mg_4Ni layer is that it be somewhat amorphous in structure in order to enhance hydrogen diffusion kinetics. Sputtering lends itself to this because of the non-equilibrium manner in which targets are bombarded with high energy plasma to deposit on another surface. Sputtering is also good because the metal layer should not react with the polymer layer underneath, which makes a physical deposition method such as sputtering is better than chemical deposition. We can also deposit thin layers with good control in a sputtering process, which we needed to do to deposit 4nm of Pt. The staff of the Fablab provided Ni, Pt and Mg targets, and we carried out the procedure with all three targets loaded in the machine to deposit in one sitting. First, we needed to deposit Mg_4Ni, and we maintained a sputtering power ratio of 1.88:1 for Mg:Ni., which is reported to give the correct composition of the alloy.[2] The Pt layer we deposit with a thickness of 4nm protect the film from oxidation and enhance the kinetic diffusion rate for hydrogen.
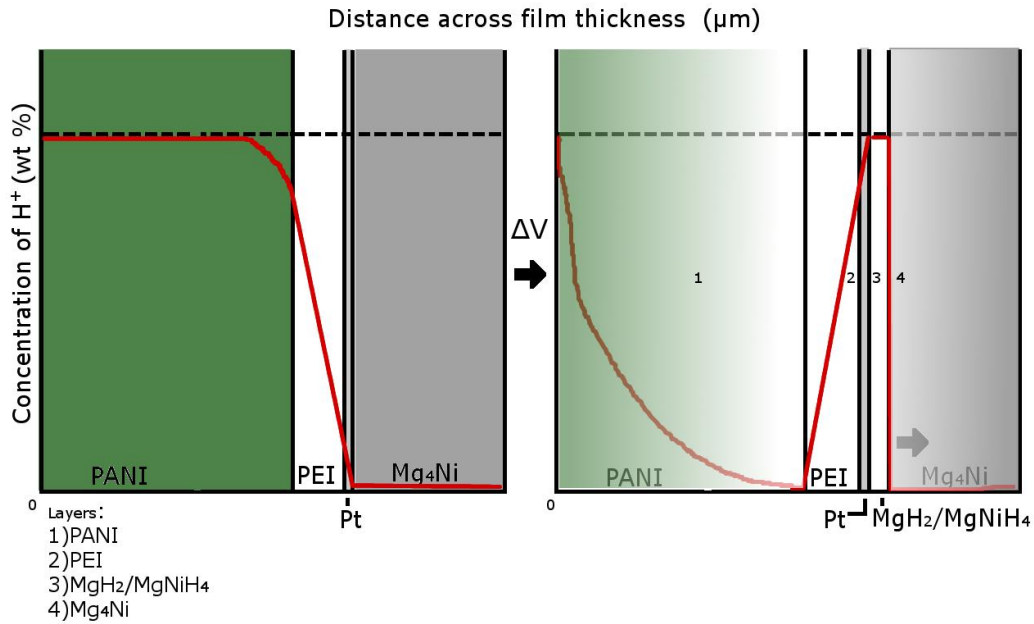

Modelling and Calculations
Electrical Analysis

The electrical analysis we developed focused on predicting a reasonable minimum operating voltage of our device and the switching time under that applied voltage. It is known that the kinetics of hydrogen diffusion play a limiting role in the switching time of Mg_xNi[5,8] and PANI[1,4] devices, which lead us to believe a model of hydrogen diffusion for the three materials Mg_4Ni, PEI, and PANI could allow us to predict the switching time of our device. Figure 3 shows a conceptual diagram of the diffusion process. We assumed that the flux of hydrogen is constant under a constant applied potential, which allowed us to use Fick's first law to model the diffusion:

$$J_i = -D_i \frac{\partial V}{\partial x} = D_i \cdot E_i \tag{1}$$

where *i* denotes the *i*th *material, J* is the flux of hydrogen, D_i is the diffusivity of hydrogen, *E* is the electric field applied determined by the voltage. Because the voltage applied will be constant, the electric field can be determined by looking at the fraction of the voltage applied on the material, determined by its thickness, over the thickness of the material. This must be multiplied by ε_r, the dielectric constant of the material, to correct for the influence of charge within the material. Flux is normally in units of mol/m^2s,

which can be obtained if we treat the diffusivity as a specific parameter for the conductivity, or mobility, of hydrogen through that material. This gives us

$$J_i \left(\frac{mol}{m^2 s} \right) = (?) \sigma_i \frac{V_{app} \cdot \frac{d_i}{d_{total}}}{d_i} \cdot \varepsilon_r \left(\frac{V}{\Omega \cdot m^2} \ or \ \frac{C}{m^2 s} \right) \tag{2}$$

where V_{app} is the thickness applied at the electrodes, d is the thickness of the layer under question, d_{total} is the collective thickness of all layers under the applied voltage, and units are in parentheses. To convert from units of Coulombs to that of moles, we must consider the collective charge for a mole of hydrogen atoms:

$$J_i = \frac{\sigma_i \cdot V_{app} \cdot \varepsilon_{r,i}}{d_{total} \cdot \mathfrak{F}} \tag{3}$$

where $\mathfrak{F}$ is Faraday's constant.

It is natural to assume that the time for a certain amount of material to pass through an individual layer will be inversely proportional to the flux of hydrogen through that material. The amount of material passing through a layer will be the areal molar concentration of hydrogen, which can be calculated by multiplying the volume density of hydrogen by its thickness, and dividing by its molar weight. This ultimately leaves us with:

$$t_i = \frac{d_i \cdot \rho_i \cdot n_i}{J_i m_{w,i}} \tag{4}$$

where t is the time it takes for hydrogen to pass through the material, ρ is the density of the material, m_w is

Figure 3 This is a conceptual diagram for hydrogen diffusion through our material. The red line shows the concentration of hydrogen along x thickness of our device. After applying a voltage, hydrogen should move out of the PANI layer, through the PEI electrolyte and Pt catalyst, and into the Mg$_4$Ni. This forms a moving front of MgH$_2$/MgNiH$_4$, a transparent insulator. We believe hydrogen diffusion through either PANI or MgH$_2$/MgNiH$_4$ limits the rate of diffusion and thus the switching time.

the molar weight of the material, and n is the number of moles of hydrogen per mole of material.

Taking all of these things into consideration, we arrived at an expression which may predict the total switching time of the material. Assuming that one layer is rate-limiting, the switching time will be the maximum of all time contributions for each layer:

$$t_{swtiching} = \max(t_1, t_2, \ldots, t_n) \tag{5}$$

In completing the electrical analysis, we also noted that an explicit amount of hydrogen is needed in order to convert a V volume amount of Mg_4Ni into $MgH_2/MgNiH_4$. At least this amount of hydrogen in the doped layer of PANI must be present in order for the device to make a complete transition. This makes the thickness of our PANI layer dependent on the thickness of our Mg_4Ni alloy. To determine the relation, we needed to compare hydrogen densities in both materials:

$$N_{H,MgH_2/MgNiH_4} = \frac{d_{MgH_2/MgNiH_4} \cdot A_{device} \cdot \rho_{MgH_2/MgNiH_4} \cdot n_{MgH_2/MgNiH_4} \cdot N_A}{m_{w,MgH_2/MgNiH_4}} \tag{6}$$

$$N_{H,PANI} = \frac{d_{PANI} \cdot A_{device} \cdot \rho_{PANI} \cdot n_{PANI} \cdot N_A}{m_{w,PANI}} \tag{7}$$

where N_H is the total number of hydrogen atoms in that particular layer, A_{device} is the area of each layer and n is the molar conversion for hydrogen atoms per moles of that layer. Equating the two equations allowed us to solve for the required thickness of PANI in terms of the thickness of $MgH_2/MgNiH_4$, which is 31% thicker than the thickness of the Mg_4Ni layer, due to volume expansion upon hydrogen intake:[8]

$$d_{PANI} = \frac{1.31 \cdot d_{Mg_4Ni} \cdot \rho_{MgH_2/MgNiH_4} \cdot n_{MgH_2/MgNiH_4} \cdot m_{w,PANI}}{m_{w,MgH_2/MgNiH_4} \cdot \rho_{PANI} \cdot n_{PANI}} \tag{8}$$

We relied heavily on equations (4), (5), and (8) in predicting the properties of our device, which meant we needed to find hydrogen conductivity and dielectric properties for each layer ourselves. The densities, molecular weighs and molar conversion had reference values we found online.

Optical Analysis

Our goal in performing an optical analysis was to accurately predict transmittance and reflectance values for our proposed device in "on" and "off" states. We acquired a floating license for the use of COMSOL Multiphysics 4.4, along with the additions of the Wave Optics Module, RF Module, and the Structural Mechanics module to aid us in this endeavor.

Performing an optical analysis necessitated acquiring complex indices of refraction for each material we planned to use. We were not able to obtain values of the indices of refraction for most of our materials during this our preliminary literature search early in the semester, and, as such, we were faced with the task of characterizing this value for each layer ourselves. However, this posed new difficulties, and for most of our modelling, we decided to use estimated values for index of refraction based on values for similar materials.

In modeling optical properties, we first performed simple verification of the software by finding the value of the Brewster angle of glass and comparing the results to the theoretical value. Following some of the provided documentation of COMSOL, we were able to model a plane electromagnetic wave propagating through free space (air) which is then partially reflected and partially transmitted through a dielectric medium (glass). We assume the field to be p-polarized, so that the electric field vector is in the same plane as the Poynting vector and the surface normal. We also assumed a periodic boundary condition that is applied on the top and bottom of the geometric model boundaries. The boundary condition assumes the solution to the electric field equations used in COMSOL is periodic along the interface between the glass and air. The reflectance and transmission equations we used are given below, which are essentially the Fresnel equations. The reflectance and transmission equations are given in terms of s-polarization and p-polarization of a plane wave.

$$r_s = \frac{n_1 \cos\theta_{incident} - n_2 \cos\theta_{transmitted}}{n_1 \cos\theta_{incident} + n_2 \cos\theta_{transmitted}} \tag{9}$$

$$t_s = \frac{2n_1 \cos\theta_{incident}}{n_1 \cos\theta_{incident} + n_2 \cos\theta_{transmitted}} \tag{10}$$

$$r_p = \frac{n_2 \cos\theta_{incident} - n_1 \cos\theta_{transmitted}}{n_1 \cos\theta_{transmitted} + n_2 \cos\theta_{incident}} \tag{11}$$

$$t_p = \frac{2n_1 \cos\theta_{incident}}{n_1 \cos\theta_{transmitted} + n_2 \cos\theta_{incident}} \tag{12}$$

Reflectance and transmission are defined as:

$$R = |r|^2 \tag{13}$$

$$T = \frac{n_2 \cos\theta_{transmitted}}{n_1 \cos\theta_{incident}} \cdot |t|^2 \tag{14}$$

The Brewster angle, where $r_p = 0$, is:

$$\theta_B = \tan^{-1}\frac{n_2}{n_1} \tag{15}$$

The model confirmed the analytical value of the Brewster angle by measuring the reflection and transmission coefficients of a plane wave transmitted through the model versus the angle of incidence. An example of the magnetic field passing through the model is shown in Figure 4. We applied the necessary boundary conditions, and compared the direct solver's solutions we applied in COMSOL to the result from solving the Fresnel equations analytically. Our results for this model are shown below in Figure 5, and the calculation agrees with the analytical value, with the Brewster angle to around 1 radian, approximately 57 degrees.
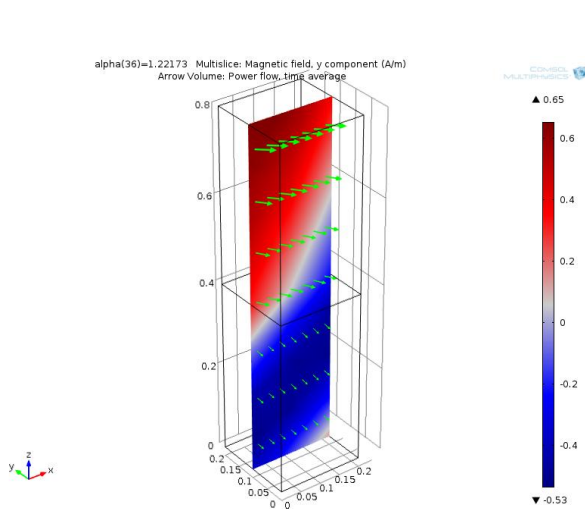

Figure 4: Y-component of the magnetic field distribution and power flow arrows for the magnetic field incident at 70 degrees
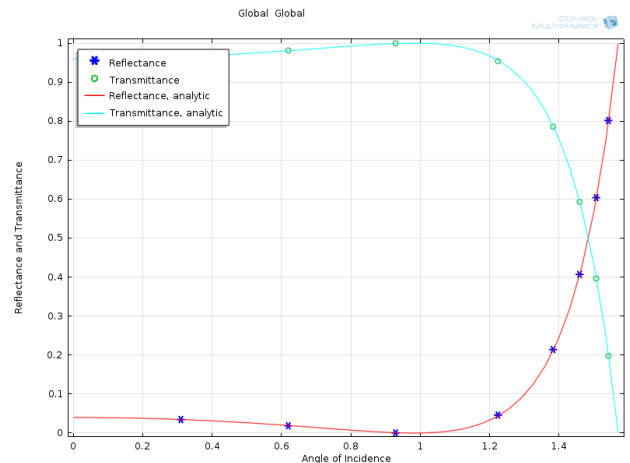

Figure 5: Reflectance and transmittance for the Y-magnetic field, which agree with the analytic values found by the COMSOL solver. The Brewster angle, where reflectance is zero, is shown to be at the value of 1 angle of incidence, which corresponds to about 57 degrees.

After verifying the Brewster angle through COMSOL, we started modeling our own device by taking a 2D geometry of our device, consisting of glass, air, polymer and platinum. We then qualitatively looked at a beam of light transmitted through our material layers. We used a Gaussian form for a transmitted beam operating on the fundamental transverse node. The plane wave is the simplest solution to Maxwell's equations. The expression of the electric field relative intensity for the Gaussian beam on the focal plane simplifies to:

$$E(y) = e^{(-\left(\frac{y}{w}\right)^2)} \tag{16}$$

where y is the center line of the beam, and w is the beam waist distance.

We planned to make changes to this model, where we make a more advanced and accurate 3D model of our device, and instead of analyzing transmittance and reflectance vs. angle of incidence, we would analyze transmittance and reflectance vs. wavelength/frequency. Unfortunately, trying to figure out how to properly compute our 3D device model with transmittance vs. wavelength frequently ended up with error messages for using too much memory. Typically we were only able to output one transmittance and reflectance value for a certain wavelength.

Our efforts using 3D models were not getting us results, so we decided to continue our work with a 2-D model, to verify it with simple models, and to implement new features in the model that account for roughness between our layers. We use the Gaussian form specified in (#) for a transmitted beam operating on the fundamental transverse node, taking a wavelength of 900 nm propagating in the x direction through our material.. We use w = 3500 nm as the beam waist, and the y = 0 as the centerline of the beam. We changed the wavelength to 900 nm so that we may be consistent with our characterization methods on our device, which analyzed our device at 900 nm.

To verify our 2-D modelling in COMSOL, we were advised to look at the transmittance through a simple thin film. We chose to look at a thin film of silver. We developed a simple 2-D model in COMSOL of an air-silver-air model, with the silver thickness at 4 nm. We used roughly the same Gaussian beam type excitation through the 2-D model as explained above. We show the figure of our silver thin film with the beam transmitted through it below.
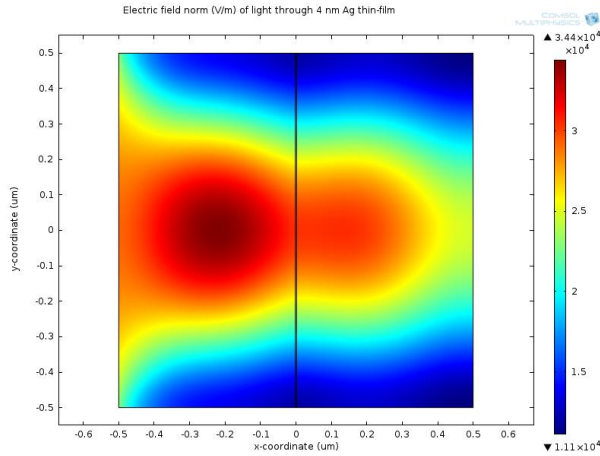
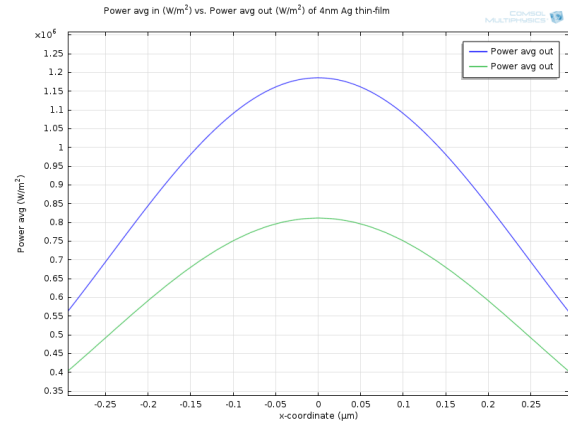**Figure 6**: Transmitted beam of light though a 4nm thin film.

Figure 7: Transmitted beam power average in and power out for 4 nm silver thin film. We see a transmittance of around 66 %, which is close to the analytical value of approx. 73%.

We see that our thin film of silver shows a transmittance of the beam of light of around 66% by taking the ratio of the green power "out" peak divided by the green power "in" peak. This agrees well with the analytical value of 73%, which we found by using the refractive index site, refractiveindex.info, which referenced Rakic et al. on "Optical properties of metallic films for vertical-cavity optoelectronic devices," from 1998.[9] We felt that this verification was sufficient to continue modeling our device in this 2-D method.

While using this method, we also frequently compared our values with known analytical values found from the literature in addition to simple calculations for transmittance we made ourselves using transmittance equation from Callister on <u>Fundamentals of Materials Science and Engineering: An Integrated Approach</u>.[10] The transmittance equation is as follows, where I_T is the transmitted intensity, I_0 is the incident intensity, l is the thickness, R is the reflectance, and β is the absorption coefficient.

$$I_T = I_0 \, (1 - R)^2 e^{-\beta l} \tag{17}$$

We also made use of refractiveindex.info, which references journal articles of material constants for optical constants and calculates transmittance values and reflectance values as a function of wavelength and frequency for a select group of materials. This site came in handy for making quick checks and for finding some material constants for use in COMSOL. We also made our own Matlab scripts to help us calculate transmittance values for ourselves.

We then added features in our model that accounted for the possible optical losses due to layer roughness inherent in our device. We implemented transition boundary conditions in COMSOL, which were based off an Effective Medium Theory incorporating values of roughness at each interface our

layers. According to Liu and Schmitt's paper on Effective Medium Theory,[11] each individual layer of our device will influence the light wave differently, and we needed to pay attention to the effects of roughness on the nanometer scale. The Effective Medium Theory can be applied to many models, and in most cases involves averaging procedures to describe a material as an 'effective' composite material. At each layer interface, there is roughness of both materials that will affect the light wave. We decided to take our roughness measurements we found for each material via AFM, assume a 50-50 volume percent of both materials at each interface, and use the root mean square of the roughness values to gain a 'composite' roughness that were used as thickness values in our model. We applied this averaging method for both the roughness of each interface, as well as the refractive index at each interface.

We decided to apply the Effective Medium Theory in creating transition boundary conditions. This helped decrease the computing memory required for the solver analysis in COMSOL. From an article by Ricoy and Volakis on generalized transition/boundary conditions for planar multiple-layer structures, they describe standard transition boundary conditions as conditions that simulate very thin dielectric layers of material (Ricoy and Volakis, 1990).[12] These boundary conditions involve lower-order derivatives of the field components, and they imply that a field is dependent on the local properties of the material, making them sometimes inaccurate for simulating homogeneous layers. We felt that their definition agreed with our choice to use these boundaries to simulate our roughness interfaces. After considering advice given by Dr. Phaneuf –and from an article on effective optical properties of nanoporous materials—we used the Drude Effective Medium Approximation to treat our interfaces. We were able to apply our own estimates of indices of refraction and thickness based on roughness's to make our model account for optical losses due to interface roughness, as well as scattering.

We performed two simple thought experiments in COMSOL to gauge the efficacy of applying the Effective Medium Theory to our model. After researching the science behind the transition boundaries, we compared a 2-D model of a transition boundary condition layer with a 2-D model that implemented an interface boundary with thin layers that changed material constants in a step series. We also tested the Effective Median approximation we planned to use in our model by comparing one simple model of a transition boundary condition with approximated index of refraction and thickness values, to a 2-D model without the EMT approximation. Only when we included k values did we see changes in transmittance, which makes sense. This will be explained in more detail in the results section.

Results and Discussion
Polymer Synthesis

We encountered little to no difficulty synthesizing the our polymers using the methods described above. The resulting solutions are shown in Figure 8. A vial of PANI after concentration by centrifuging is on the far left. The PEDOT:PSS came suspended in H_2O, to which we added DMSO, and later methanol for enhanced wetting, shown in the center. Finally PEI is on the far right.

Figure 8: From left to right; solutions of PANI, PEDOT:PSS, and PEI

Next, we were faced with the challenge of depositing thin films for each polymer. The desired characteristics for each thin film include minimum roughness to prevent optical scattering between the layers in the final device and appropriate thickness for film resilience, optical transparency, and hydrogen storage in the case of PANI.

During the first attempt at spin coating PEDOT:PSS, it became immediately obvious that the film was not depositing evenly across the surface of the substrate. Figure 9 compares preliminary attempts at spin coating PEDOT:PSS (in blue) and PANI (in green) to the final deposition. The initial spin coated film already appeared by visual inspection to be thicker in some areas and much thinner in others, which would have caused increased scattering and ultimate failure of our device.
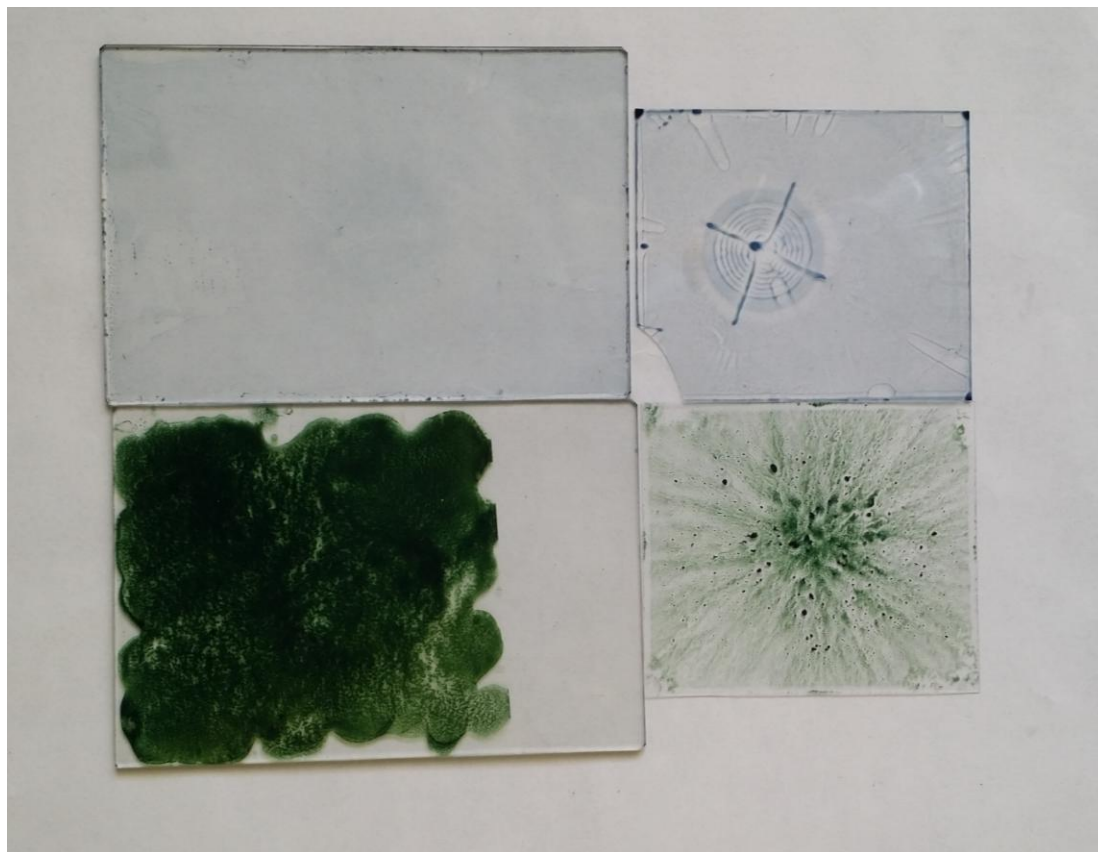
Figure 9: Comparing final depositions to the preliminary spin coating attempts on the right. Clockwise starting at top right; preliminary PEDOT:PSS deposited by Spin Coating, preliminary PANI deposited by Spin Coating, final PANI deposited by Drop Casting, and final PEDOT:PSS deposited by Spin Coating.

Due to the initial disappointment of depositing PEDOT:PSS by spin coating, we switched to Meyer Rod Deposition, another thin film deposition method. While experimenting with this method, we realized that the real issue causing the film to deposit unevenly was the hydrophobicity of the substrate, which was essentially repelling the aqueous PEDOT:PSS solution and making it difficult to wet the glass slide. Thus, we decided to add 50 vol% methanol to act as an organic solvent and coat the glass slide evenly. This was very successful, and the subsequent Meyer Rod coating is shown in Figure 10.
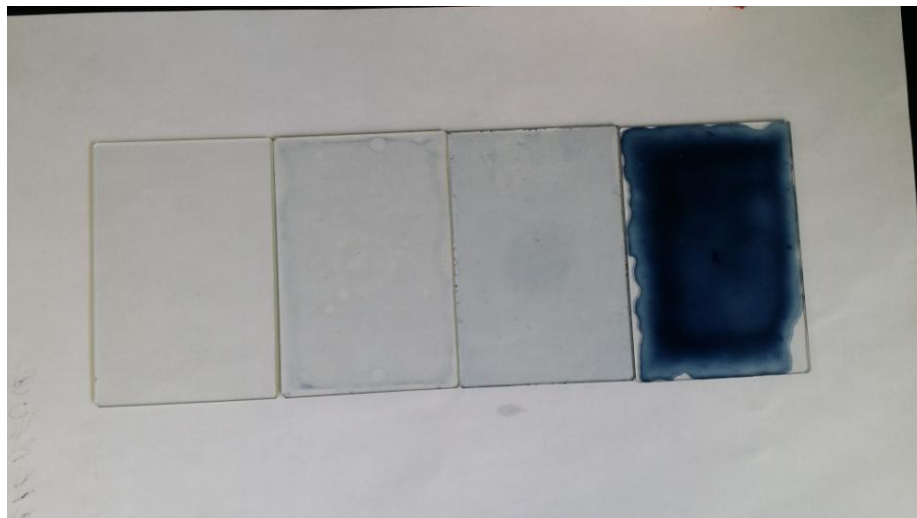
Figure 10: From left to right; control glass slide, PEDOT:PSS deposited by Meyer Rod Deposition, PEDOT:PSS deposited by Spin Coating, and PEDOT:PSS deposited by Drop Casting.

Once we figured out that the key to an even layer was the methanol solvent, we decided to return to the easier method of spin coating. After several trials, we concluded that the best film with no visual streaking was achieved using the spin coater at 2000rpm. Further along, when the first prototype was fabricated and tested, we noticed that the electrical contacts were destroying the integrity of the PEDOT:PSS film. Reported in the characterization section, the PEDOT:PSS film was very thin, only 70nm, and we eventually decided to try and deposit a thicker layer so that it wouldn't tear as easily. Based on our spin coating experience, using a slower rpm did not result in a thicker film. Therefore, we tried depositing multiple films on top of each other. These results are shown in Figure 11. The additional layers usually caused the film to break, seen on the center slide. The lack of success in this area caused us to attempt drop casting on PEDOT:PSS, seen on the far right in Figure 10. However, this causes PEDOT:PSS to lose the desired characteristic of optical transparency and therefore is not feasible. We concluded to remain with the single layer of optimum spin coated PEDOT:PSS on the far left.

Figure 11: From left to right; final spin coated PEDOT:PSS film, attempt at spin coating multiple layers, and control glass slide

The first attempt at spin coating PANI is shown above on the bottom right in Figure 12. This first film has high roughness and is very uneven, some parts of the slide still entirely exposed. Since the PANI did not seem to be able to cover the entire slide, we decided to try concentrating the solution using the centrifuging method. We also had to ultrasonicate the concentrated solution to help break up the agglomerations of polyaniline and achieve a more uniform coating. This was successful using the same spin coating settings as with PEDOT:PSS, shown on the center slide in Figure 12. However, in order to balance the hydrogen mass according to the calculations in the electrical modeling section, the PANI layer had to be at least a micron thick. As detailed later in the characterization section, the Mg_4Ni layer was thicker than expected, requiring more hydrogen source from the PANI film. We discovered that the final film would need to be two microns thick in order for the device to fully switch, which would require approximately 30 layers of the 70nm spin coated PANI film. Consequently, even though spin coating deposition method achieves a smoother, more uniform layer, we had to stick with the rougher drop casting method in order for our device to work in the limited time frame available to us. Not only does drop casting yield much rougher films than spin coating method, potentially causing unwanted optical scattering, it is also too thick for all of the hydrogen to fully diffuse out and the PANI to switch to its transparent state. In this case, we opted for too much being better than too little.
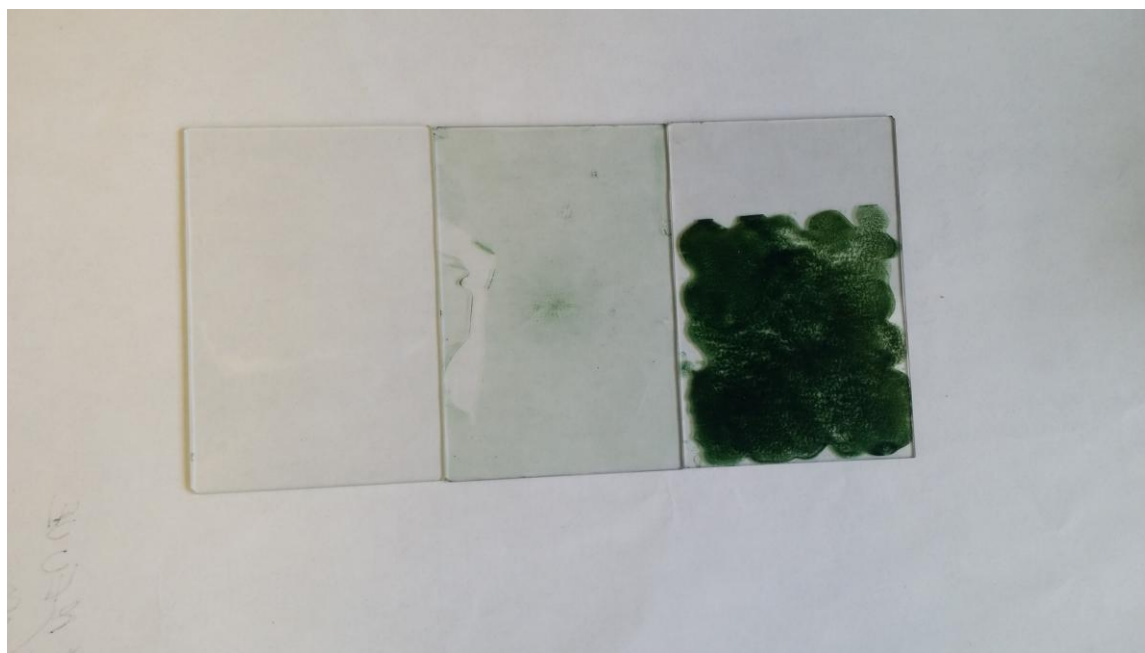

Figure 12: From left to right; control glass slide, PANI deposited by Spin Coating, PANI deposited by Drop Casting

The PEI layer was the simplest to initially deposit a prototype film. PEI did not have any problems wetting to the glass substrate because it was already dissolved in an organic solution of gamma-butyrolactone. Since PEI is used on the device by spin coating on top of PANI we had even less of an issue with wetting by combining two organics. Using a slower rpm than PEDOT:PSS due to PEI's higer viscosity, it was evenly spin coated at 500rpm. The resulting film is demonstrated in Figure x, the second from the right, and easily held our device together after curing. However, the unusual hydrogen diffusion

behavior exhibited by our device can be linked back to the thin PEI film possibly being damaged and further analysis would have to be done to deposit a more resilient electrolyte.

The results from the final thin film deposition methods used for the device are shown separately on different slides for comparison in Figure x. The sputtered Pt on Mg_4Ni is shown on the far left and will be discussed in the next section. The next slide has a sample of drop casted PANI, showing the thickness and probable roughness of the layer. The middle slide has the final PEI thin film, spin coated at 2000rpm for a layer about 70nm. The resulting layer is very even. PEI, the second from the right, is hard to tell because it is also transparent but it was by far the easiest to spin coat and was deposited at 500rpm. The last slide is blank for comparison.

Figure 13: From left to right; Pt on Mg_4Ni, PANI, PEDOT, PEI, and control slide

Sputtering

We sputtered our Mg_4Ni/Pt layers onto four different substrates, two with PEDOT:PSS on glass and two just on glass, using the AJA Sputtering Unit at the Maryland Nanocenter. We weren't able to use the exact operating conditions Tajima's group used due to differences in the sputtering machines between our two groups. Tajima's group operated at a base pressure of $1.4*10^{-7}$ Torr, with a working pressure of 2 mTorr, a target-to-substrate distance of 100 mm, and they sputtered Mg at a power of 22 W and Ni at 11.7 W. Doing so, they deposited a 50 nm layer at a rate of 0.8 nm/s.[5] Under the advisement of a lab technician at the Maryland Nanocenter, our set-up used a base vacuum pressure of $2*10^{-6}$ Torr, a working pressure of 7.5 mTorr, a target-to-substrate distance of 110 mm, and we set a sputtering power of 200 W for Mg and 105 W for Ni.

We believed maintaining the same power ratio between the Mg and Ni targets as Tajima's group used would yield the same composition alloy. In order to achieve an even composition profile, we also rotated our substrates throughout the process. We sputtered 200 nm after 12 minutes, as determined by profilometry, meaning our process, despite the higher power, had a deposition rate of 0.28 nm/s. Unfortunately, we were only able to schedule one sputtering session within the timeframe of the semester,

but knowing the rate of deposition based on these sputtering conditions would allow us to tailor the thickness of Mg_4Ni in future sputtering sessions. After sputtering on the Mg_4Ni layer, we then capped the layer with 4 nm of Pt, sputtering the Pt at a power of 200 W for 8 s, at a rate of 0.5 nm/s.

Figure 13 shows what our films looked like after our sputtering session. We were pleased that the films adhered nicely to the polymer films, and a visual inspection from the backside of the glass did not show any inherent roughness or damage to the underlying PEDOT:PSS.

Finished Device

The finished device is shown after testing in Figure 14. It is placed above an Mg_4Ni film for comparison of what it looked like before the hydrogen diffusion took place. The dark square shows where the hydrogen has diffused into the Mg_4Ni layer, causing it to no longer be reflective. The PANI, however, is too thick to reach its transparent state and the reflective magnesium alloy surface simply becomes dark. In future iterations of the device, it would be imperative to deposit PANI at just the right thickness for the transition to occur, and also in a different deposition method that leaves behind a flatter film.
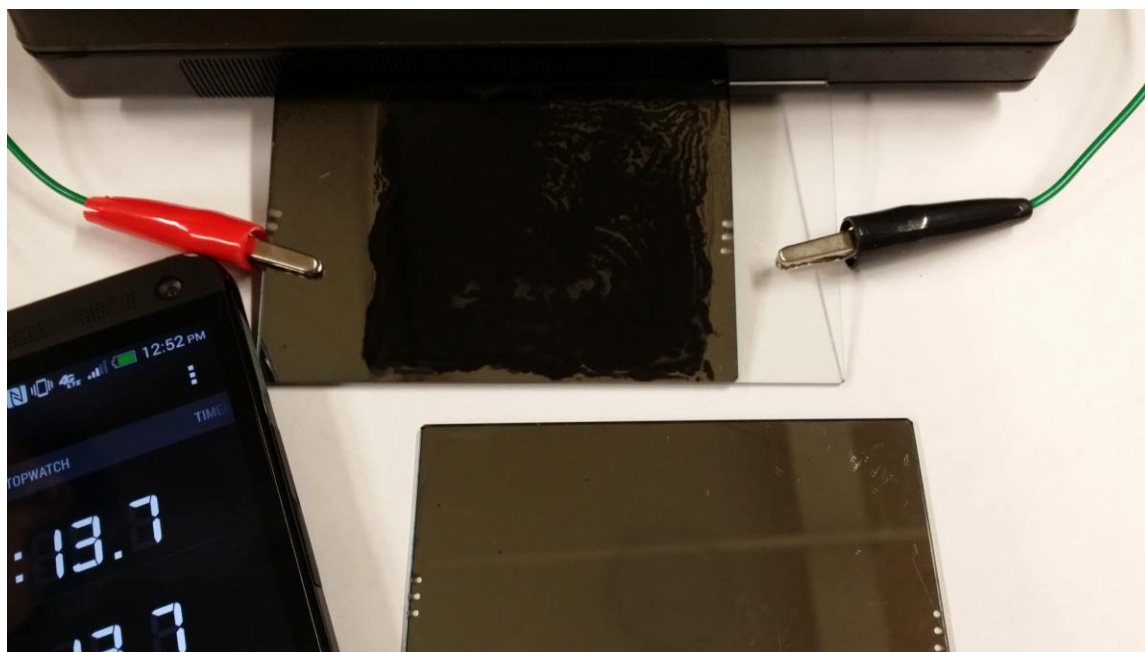

Figure 14: Final device on testing apparatus, compared to Mg_4Ni film before testing below.
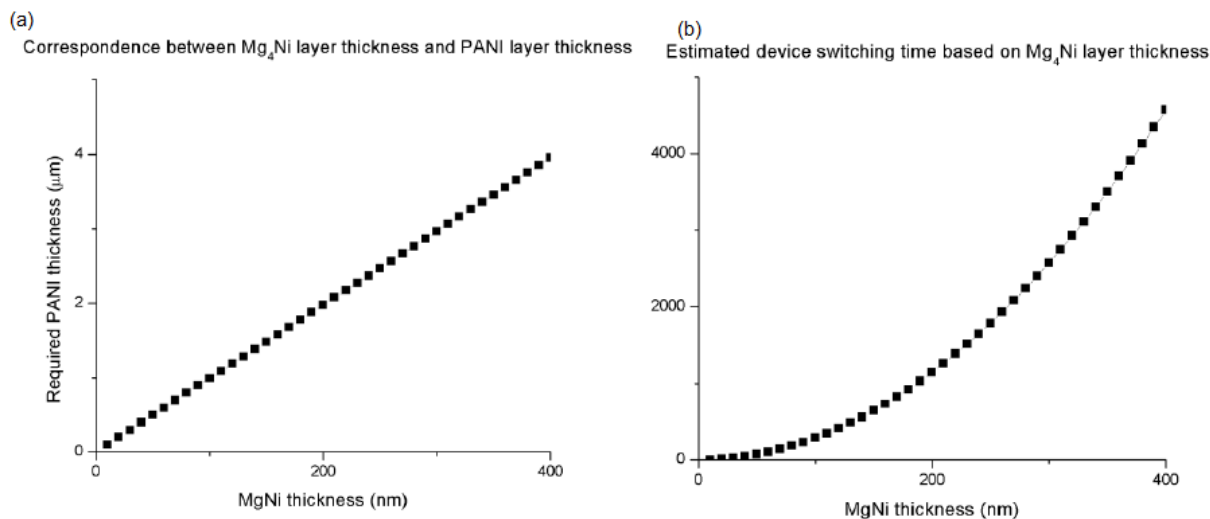
Figure 15: These are plots obtained based using equations (8) and (5) to find (a) the required thickness of PANI based on Mg_4Ni thickness and (b) the switching time dependence based on Mg_4Ni thickness. Although we determined Mg_4Ni has lower hydrogen conductivity than the PANI, the fact that the PANI layer is so much thicker makes it rate-limiting in our predictions.

Electrical Predictions

The eventual expression we arrived at in eq. (5) requires the knowledge of several materials parameters for each layer under the applied voltage. These layers are PANI, PEI, Pt, Mg_4Ni, and the resultant $MgH_2/MgNiH_4$ which grows from the solid-state reaction. Many of these parameters are unknown and thus require specific characterization, so we made some simplifying assumptions based on the system in question for preliminary predictions.

The first assumption we have made is that one material will likely be rate limiting in the hydrogen transfer process, and thus its time contribution to the switching time will dominate over all others. Considering the materials within this system, we believe either the $MgH_2/MgNiH_4$ or PANI will be rate limiting, due to the fact that MgH_2 is reported as rate limiting the kinetics for hydrogen absorption and desorption in Mg-storage systems and PANI is known to have slow switching speeds for large layers.[8,9,**] PEI is reported as a hydrogen electrolyte, which we believe makes it much faster at transporting hydrogen than the other layers.

We then assumed that if this would be the case for our system, it is likely the case for Tajima's system or past devices made with PANI. Tajima reported an "on" switching time of 30s for a device consisting of $ITO/WO_3/Ta_2O_5/Al/Pt/Mg_4Ni/ITO$ under an applied voltage of 5V. They used a 50nm layer of Mg_4Ni, and 400nm layers of WO_3 and Ta_2O_5.[2] From a review of the electrochromic properties of PANI,[4] the authors reported a switching time of 9s for a 320 nm film under an applied voltage of 1.2V. With this data, and taking the dielectric constant of $MgH_2/MgNiH_4$ and PANI to be the square of their indices of refraction, we were able to calculate the conductivities of the materials to be about $1.32*10^{-8}\,\Omega^{-1}cm^{-1}$ and $3.2*10^{-8}\,\Omega^{-1}cm^{-1}$, respectively.

Knowing the conductivities, we used equations (5) and (8) to generate the plots shown in Figure 15, which show the dependence of both PANI layer thickness and expected switching time of the device as a function of how thick a Mg_4Ni layer is deposited. These diagrams gave us specific dimensions to aim for in making a device with a switching time of 30s: ~35nm for Mg_4Ni and 400 nm for PANI. Our device

had a 200 nm layer of Mg_4Ni deposited, which means the required PANI thickness for our device is ~2 μm and predicted switching time is 1143s.

For our glass slides, which are 3" x 2", we can also predict a current under an applied 5V using equation (2) by multiplying the anticipated current density by the area of the device. This gives a prediction of 14.0 mA.

Optical Predictions

We wish to present the results of our optical modeling through multiple approaches, software and calculations. The goal is to gain a reasonable understanding of how our device might operate as a transparent window. In COMSOL, this means looking at the electric field intensities, power output and refractive indices through the device layers. We did not try to model the reflectivity of the device in its off-state because the more relevant challenge for any smart window device is to turn transparent in the on-state. An even greater and more elaborate challenge is to then make the device turn from reflective to transparent, reversibly. This last criterion we did not capture through our modelling; we focused on doing calculations for an ideal scenario.

Our group used COMSOL to solve Maxwell's equations in the frequency domain, a time-independent domain, using a finite element method. We focused on creating thought-experiments and approximations of the device when fixed in the transparent state with a particular frequency of light propagating through it. After working with the software and reviewing past work, we developed a better understanding of how we might want to model the device using other domains and techniques, which could be used in future calculations. As is, the frequency domain allowed us to calculate the electric field intensity and power output at a number of finite elements within the representative geometry for the device. By normalizing this over the inputted power or electric field we could get an approximate light intensity or transmittance for our device.

This method required a handful of assumptions as a result of minimal experimental data available within the literature. Certain assumptions will be discussed on a case-by-case basis but other factors, such as unknown material properties needed to be resolved immediately to create our model. In particular, the indices of refraction for two materials needed to be estimated completely because they were either unknown and/or scarcely found in the literature. While this error in our model does directly impede the accuracy of our results, it is also a testament to the novelty of our approach and design. Our team was limited in both time and the amount of measurements we could make, so these values were taken from the literature or estimated from other similar experiments. If given more time, one of the first concerns of this modeling team would be to test components of the finished device for optical properties and measurements.

Specifically, the PANI layer we use in this design gives up hydrogen atoms in its polymer chain which diffuse through the device and into the metallic Mg_4Ni layer. This mechanism creates a new $MgH_2/MgNiH_4$ hydride composite and a PANI layer deficient of hydrogen, both with unknown optical properties. Our team did not have enough time to measure the indices of these materials after a final prototype had been made and tested. Ideally, each intermediate layer between the PANI and Mg_4Ni would also be tested due to any cation doping transitions or effects.

The complex index of refraction for multiple layers in our device were either taken from other experiments or estimated as well. In an experiment by MO Dang et al,[13] the ellipsometric spectra and refractive index of insulating polyaniline was measured to be: n=1.51 at 632.8 nm and n=1.63 at the peak of the visible range. Even though this PANI layer was prepared differently and tested in contrasting conditions, our group took these numbers for the refractive index values for our layer. Finding a reasonable refractive index for $MgH_2/MgNiH_4$ was also unsuccessful. We had hoped that Tajima's group would mention the refractive index of their layer but instead we found few sources that even dealt with this particular material. We eventually decided to best guess values of: n=2.0+0.01i at 900 nm and n=1.4348+0.01 at 600 nm based on values for transparent glass. This change from 900 nm to 600 nm was done not only for this material but also for others that had measured indices for only 900 nm.

Unlike the other physical properties of our model, the refractive indices of any material will vary with the wavelength of propagating light. For our soda-lime glasss and thin platinum layers, the refractive indices had already been measured at every necessary wavelength. But for other materials, such as the PEDOT:PSS and PEI polymer thin films, we received our refractive indices from ellipsometer measurements done only at 900 nm. This meant that we had to perform some estimation of the change in refractive index if we wanted to design a model of our device at wavelengths other than 900 nm. When our group decided to make a model at 600 nm we took a percent change in refractive index from other similar materials and applied that ratio to our unknowns. For the two unknown polymers, PEI and PEDOT:PSS, we used the change in the PANI as a benchmark ratio for the change in PEI and PEDOT. For the $MgH_2/MgNiH_4$ refractive index at 600 nm we used the ratio from the change in platinum's refractive index and multiplied it by the refractive index of MgH2/MgNiH$_4$ at 900 nm. Though crude, these estimates were made to the best of our ability. Our group would have greatly preferred obtaining the correct values, but we were not prepared for the complexity of obtaining accurate measurements for unkown materials in the N&K spectrophotometer. A table of the final complex refractive indices used in both our final COMSOL models is included below, in Table I. Any dash in the table represents an absorption component that is negligible. This is also true of the soda-lime glass but we have included this value to show who low these values can be in comparison to metals and other opaque materials.

$$\vec{n} = n + ik = n(1 + i\kappa), \text{ where } \kappa = \text{the extinction coefficient} \tag{18}$$

Material Layer	At 600 nm		At 900 nm	
	n	k	n	k
Soda-Lime Glass[14]	1.523	4.548 E-7	1.515	3.727 E-6
PEDOT	1.525	-	1.656	-
MgNiH	1.435	0.01	2.0	0.01
Platinum[9]	2.253	3.969	3.140	5.381
PEI	1.488	-	1.617	-
PANI	1.50	-	1.630	-

Table I

The table above neglects inclusions from our treatment of the transition boundaries between different thin film layers using an effective medium theory. For this theory we calculated a number of other refractive indices that will be explained later in the results.

The geometry of each simulation in COMSOL was rendered in only 2-dimensions for added simplicity and additional computing memory. When our modelling team first started drawing up schematics of our device, we fully expected to be able to mimic the dimensions and sizing in our optical model. Yet due to the finite and sometimes limited memory available within our computer, we made certain compromises with our geometries. In particular, we were having recurring difficulties computing a model with two full layers of our soda-lime glass. With a thickness of 1,100 microns, these slides were immense compared to every other layer in the stacked geometry. As a result, our standard meshes became microscopic at each interface and required too much memory to compute. When we tried other tailored and uneven meshes, we started to compromise the accuracy of our model. To avoid this problem, we walked through a thought-experiment to test a simplified geometry by hand. Our group calculated the difference between the transmission through 1,100 microns of glass, and then through 1 micron of glass. We found a difference of around 1% in the two transmission values and decided this was sufficiently small difference to improve the overall performance of our design. This quick calculation used **Equation #** which has also been incorporated into a script of Matlab code for faster results. Our thinner glass layer was still able to use the sample end roughness measurements so we did not greatly impact any of the interfaces in our simulation. The final dimensions of our geometry were therefore on the micron scale

with nine layers to include Air-Glass-PEDOT-MgH$_2$/MgNiH$_4$-PEI-PANI-PEDOT-Glass-Air. This layout also includes transition boundaries in between each layer which incorporate roughness through the effective medium theory and a thin platinum layer. Our team also added a polygon with points through the center of the design to look at transmittance of the device in 1-dimension. These segments also show up in our simulation are a separate shape from the most obvious rectangle, as seen below. A picture of our completed geometry is included below, in Figure 16.

Figure 16

      All of the edges and interfaces in our geometry required special treatment in our simulations. Our modeling team mimicked other designs by including only a single port for wave excitations on one side of our device and then scattering boundaries around the rest of the edges. All of these scattering boundaries are treated as first-order absorbing electric boundaries for a plane wave. This suits our simulation well since we have designed our plane wave to have negligible interactions with the edges of the geometry. Another option would have been to use a perfectly matched layer at our edges. This is a domain feature rather than a boundary condition because it simulates an infinite domain where any wave can propagate and disappear without being reflected back. We compared both features in our preliminary models and did not notice any substantial differences between the two.

      Our port on the left-side of the simulation is the sole source of wave excitation. The port emits a plane wave that starts at the (-3.75, 0, 0) coordinates then propagates along the positive x -axis. We were able to control the angle of propagation, the width, and the power of the plane wave in COMSOL. We wanted the wave to intersect each of our device layers orthogonally and have a small enough width which does not interact with the edges of the geometry. We did, however, encounter a problem encountered related to the phase of the wave. We realized we could greatly impact the electric field interactions at each interface in our device by varying the phase or size of our air layers. This became an issue since most of our measurements for transmission looked at the electric field and power at each interface. Due to variations in the phase, frequency or thickness of our air layer, our results tended to vary in a way we could not anticipate. To maintain consistent calculations, we varied the thickness of our air layer and its phase degree to match our other samples. Whenever possible, we tried to make sure the electric field of the plane wave was at a maximum when it interacted with the first air-glass interface. This consistency helped us produce more uniform results when we looked at multiple frequencies propagating through our sample.

Our group also had to assess whether roughness at interfaces, which we modeled through transition boundaries, were crucial to the validity of our model. These transition boundaries are either our thin platinum layer or the roughness between each layer into our simulation. We calculated independent complex refractive indices at each transition boundary using effective medium approximations to describe the interactions between the materials at an interface. Effective medium theories yield dielectric functions of composite media which directly relate to complex indices. These types of approximation treat each interface as a composite material layer with thickness equivalent to interface roughness. For our model, we used the Drude effective medium approximation to calculate the refractive index. This equation, presented as

$$n_{eff}^2 = (1 - \phi)n_c^2 + \phi n_d^2 \tag{19}$$

where n_{eff} is the effective index, n_c is the index of refraction of one layer, n_d is the index of refraction for the other, and ϕ is the volume fraction, is known to over predict the index of refraction of thin films, but we found its simplicity adequate for our rough interfaces. Other approximations that we did not have enough time to look at include the Maxwell-Garnett theory, Bruggeman, Lorentz-Lorenz and the volume averaging theory ((VAT), which all could have been used to calculate a refractive index.

The corresponding interfaces created from the effective medium approximation can also be added to our table of refractive indices. This table can be found below and also include the thickness of each layer. We ignored the adsorptive component of the refractive index because of the thin nature of each interface. The thickness of the interface relates directly to the roughness of our samples. Some of these thicknesses were added together as the layers of the device are stacked on top of one another. Any change in roughness due to the sandwiching of our two glass slides to make the finished prototype is not taken into account by our COMSOL simulations. We split all of the volume fractions equally between both materials at an interface.

	At 600 nm	At 900 nm	Thickness
Material Layer	***n***	***n***	*(nm)*
Air and Glass	1.284	1.284	5.27
Glass and PEDOT	1.523	1.587	5.27
PEDOT and MgNiH	1.480	1.836	7.59
PEI and PANI	1.494	1.624	12.36
PANI and PEDOT	1.513	1.643	7.59

Table II

Our team conducted a number of thought experiments to test the validity of our assumptions and choices throughout the simulation. In particular there are two recent experiments that we performed under the advisement of Dr. Phaneuf. The first experiment dealt with the treatment of transition boundaries in COMSOL. The second tested the impact of effective medium approximations on our model. In both experiments we looked at two different geometries for each case to distinguish between the results. The purpose of the first experiment was to find out how COMSOL sees a transition boundary and how many nodes or calculations it does at the interface. To test this, we created one scenario which uses a standard transition boundary of finite thickness. Then, we produced another scenario which added multiple, thin layers at the interface to step the index of refraction up from air to glass, in 0.1 increments. Both scenarios create an interface with the same thickness, but one method used a step-wise transition while the other method used the COMSOL transition boundary. The results from this first thought experiment are included below, in Figure 17. The experiment showed that the power out/in curves for these two scenarios are within less than 0.1% of each other. Thus, the difference between these two interfaces are negligible. After this experiment we did further research to figure out how transition boundaries are treated in COMSOL. We learned that while both scenarios showed an accurate transition between the glass and air layers, the transition boundary used substantially less nodes and memory to make the same calculation.

Our group felt more comfortable incorporating transition boundaries into our already hefty design. Further analysis of the effective medium approximations at our rough interfaces were treated in this paper's second thought experiment.
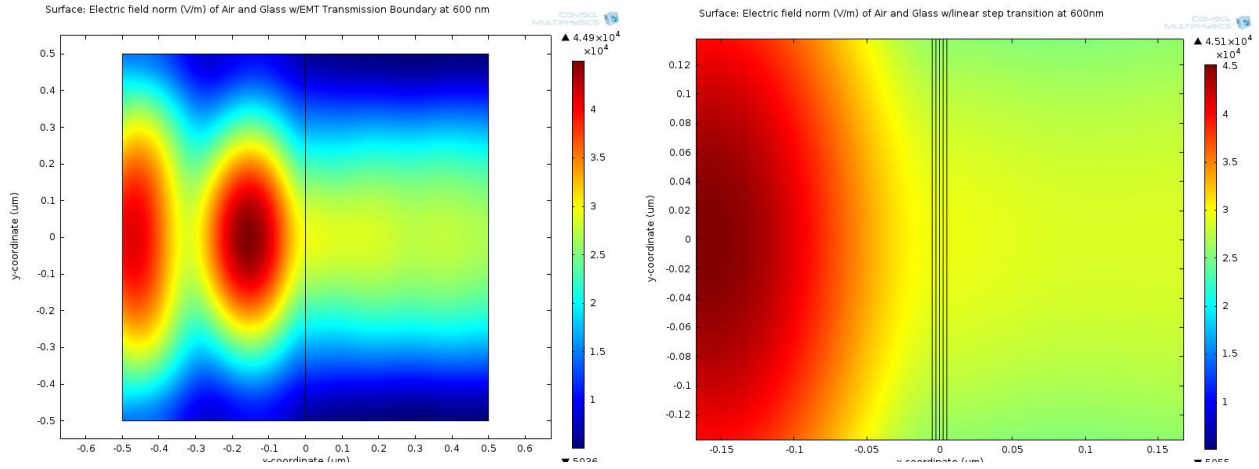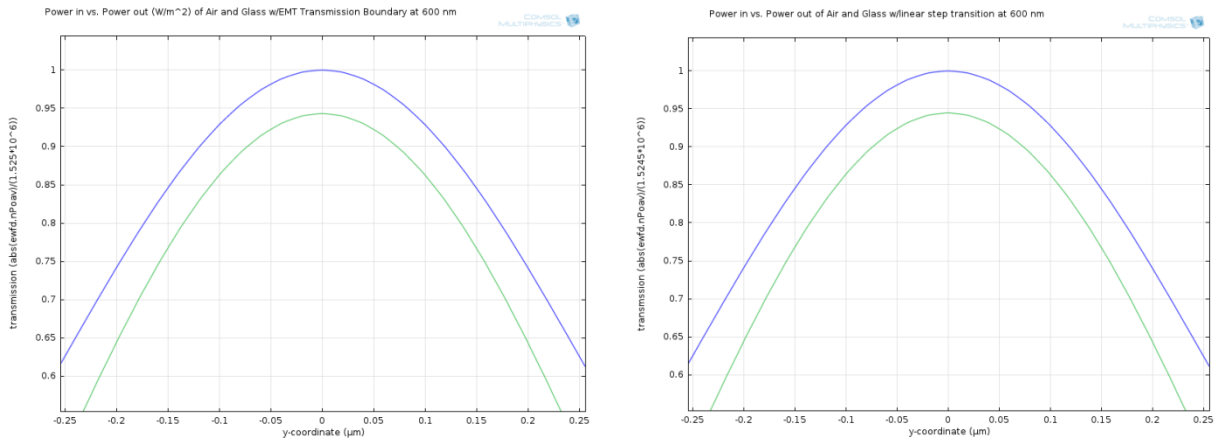

Figure 17: The e-fields from the first thought experiment to test the treatment of transition boundaries by COMSOL (a) The geometry with a transition boundary that applies the Drude EMA(left). (b) A geometry with 4 layers of equivalent size that step from one index to the next (right).

Figure 18: The transmission curves from the first thought experiment to test the treatment of transition boundaries by COMSOL (a) The geometry with a transition boundary using the Drude EMA (left). (b) A geometry with four layers that step from one index to the next (right).

This thought experiment was designed to look at the impact of roughness on an interface. We designed a geometry with and without a transition boundary between borosilicate glass and PEDOT:PSS. These materials were initially chosen because they have comparable indices of refraction to those found in our final design. Later, our team recognized both materials lack significant adsorption coefficients, and these materials were therefore not ideal in consideration of a rough or scattering interface. We determined it was likely defects, gaps and other interferences could contribute a complex absorptive component to an interface. Since this attribute was omitted in thought experiment, our group later became skeptical of the results. These other considerations were not specifically included, but they did affect our interpretation of the results. The simulation used the effective medium approximation from Drude theory to calculate a refractive index for the PEDOT:PSS and Borosilicate interface. We calculated $n_{eff} = 1.507$ assuming

that $n_{PEDOT:PSS} = 1.523$ and $n_{Glass} = 1.490$. The results for a propagating wave at 1 W and 600 nm are included below in Figures 19 and 20. These results showed power out/in curves for both scenarios, and the results were 1% of each other. Though this tells us that the transition boundary is negligible, the scenario which we modelled is too ideal for us to assume we can neglect any rough interface, and we agreed our model would be more accurate with roughness transition layers. If we had experimentally found our own n and k values we also may have accounted for adsorptive losses at each material interface to greatly improve the accuracy of our model.

Figure 19: The e-fields from the second thought experiment to test the use of effective medium approximations to model surface roughness in COMSOL (a) Is the geometry with a transition boundary that applies the Drude EMA (left). (b) A geometry without any transition boundary (right).
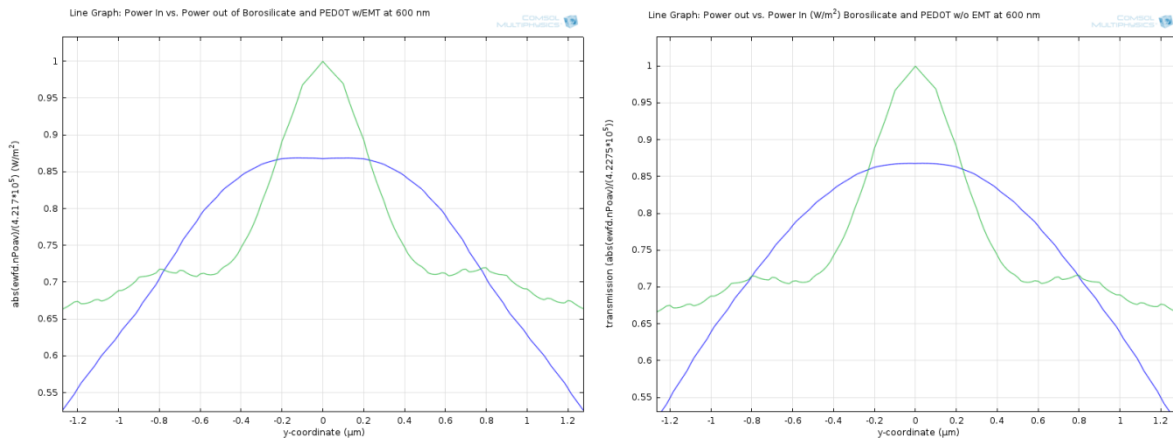

Figure 20: The e-fields from the second thought experiment to test the use of effective medium approximations to model surface roughness in COMSOL (a) Is the geometry with a transition boundary that applies the Drude EMA (left). (b) A geometry without any transition boundary (right).

The final iteration of our model considered a planar wave propagating perpendicular to the device at two wavelengths, 600 nm and 900 nm. Throughout the semester, our team created numerous models to build up to this final simulation. We periodically checked the results from our COMSOL simulations against our own calculations and Matlab script. One article provided by Dr. Phaneuf,[15] discussed the imminent effects due to multilayer internal reflections and interference in our device. While our team did recognize the importance of these calculations, we were not able to complete sufficient calculations using these sources beyond the basic Fresnel Equations, repeated for multiple surfaces. Using equation (17), our team estimated a final transmittance of 50.34% at 600 nm for our device (excluding the EMT transition

boundaries). We can compare this value to our results from COMSOL for light propagating at 600 nm and 900 nm in Figures 21, 22 and 23.
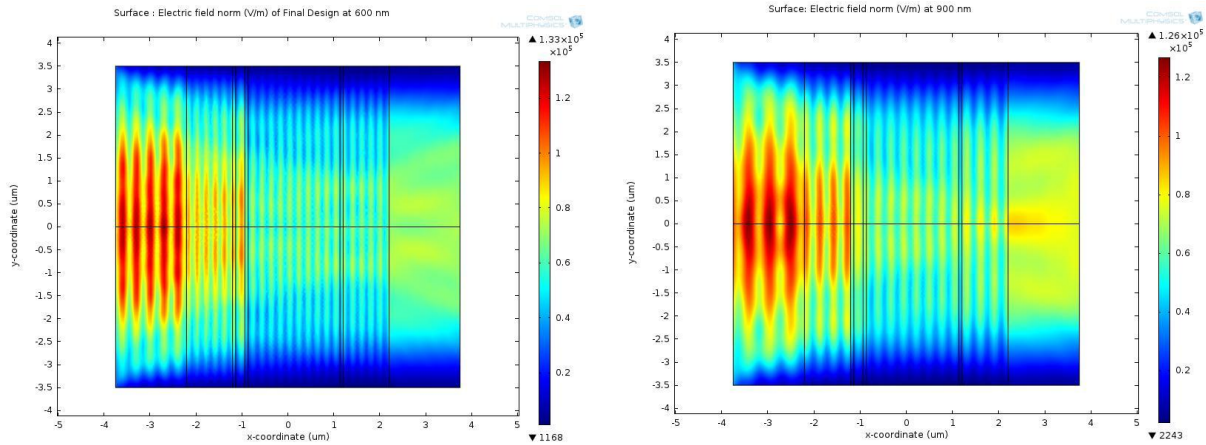

Figure 21: The e-fields from the final design with a planar wave of 60 Watts. (a) The results for the model at 600 nm (left). (b) The results for the model at 900 nm (right).
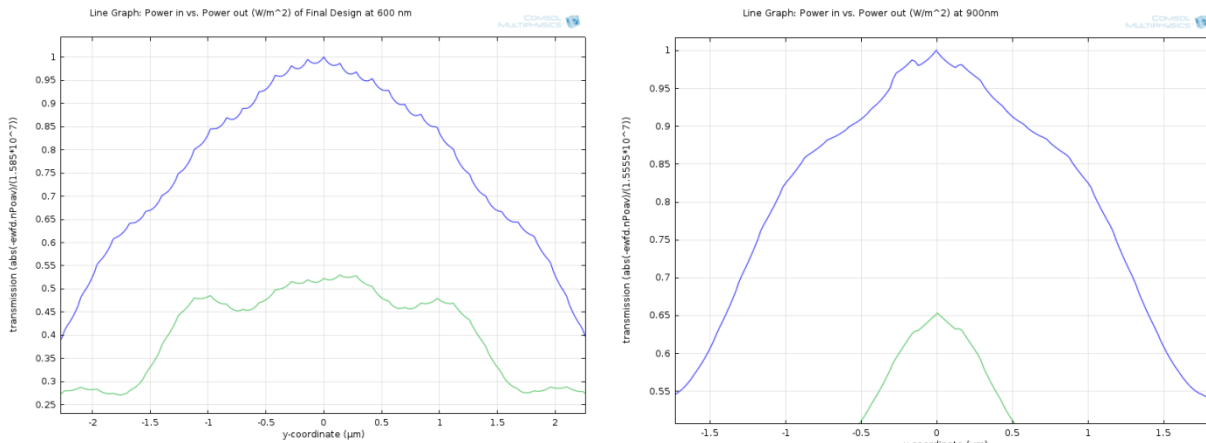

Figure 22: The power out/in curves from the final design with a planar wave of 60 Watts. (a) The results for the model at 600 nm (left). (b) The results for the model at 900 nm (right).
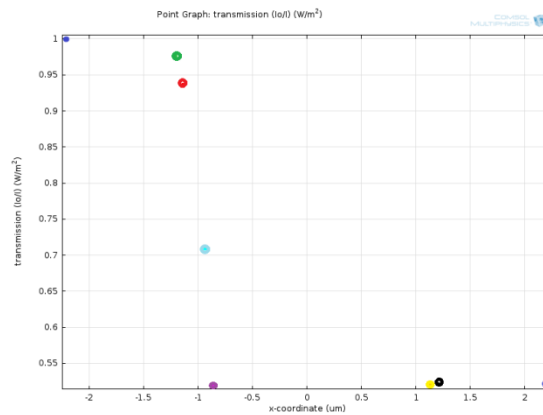

Figure 23: The point plot of our 600 nm simulation with each point corresponding to an interface on the device. Each of the points follow a line segment along the x-axis. These points show a step-wise decrease down to around 50% which mirrors our power in/out ratio in the curve above for 600 nm.

In the first pair of plots above, the figures show the calculated electric field of our geometry. The color scale for this plot is in volts per meter which is reasonable since our wave has a power of 60 Watts (a standard light bulb) and a size on the micron scale (10^{-6} m). Even on these plots our team noticed interference patterns forming in the air layer after our device. These patterns depend on the phase and wavelength of our planar wave. The next set of figures contain power out/in curves at the two glass interfaces. Some portions of these graphs have been zoomed in to better compare the resulting transmission losses. Our y-axis on these plots is the average power of the field along that interface normalized by the input power. This calculation we interpreted as the transmittance since it closely mimics the intensity out/in for our device. Both curves also show obvious interference patterns at the last glass interface, after the wave has propagated through the device. The final figure for this model is from the 600 nm simulation. This is a point plot that looks at the power out/in ratio along the x-axis of our geometry. Each point is another interface of our device and as seen, there are eight total interfaces to our final simulation. One of the major concerns with a plot like this is that each interface is not in phase with one another. This could impact the power out/in ratios that are shown in the plot. This could also explain why some of our intermediate interfaces show lower ratios than the final interface. Uncertainties like this are evidence that our team could still improve these models and our calculations for checking these COMSOL simulations. Our results from these COMSOL simulations predict a transmission of around 52% at 600 nm and around 65% at 900 nm, and the 600 nm result agrees well with 50.34 % calculated using equation (17).

Characterization

Concurrent with our modelling, we planned to do several characterization techniques in order to make our models more accurate and understand the nature of our device. First and foremost, we needed to know the thickness of each layer we deposited as we deposited it, which we accomplished by doing profilometry. In order to assess whether or not roughness might affect the results of our optical calculations, we performed atomic force microscopy (AFM). To ultimately test our device, we gained access to a power supply in Dr. Wuttig's lab along with electrical wiring equipment to properly apply a voltage across the device. Two techniques which we wanted to do, but ultimately did not pan out well, were N&K Spectrophotometry to characterize indices of refraction for each layer, and energy-dispersive x-ray spectroscopy (EDS) to confirm the composition of our Mg_4Ni/Pt layer.

Profilometry

After depositing each layer, we wanted to characterize the thickness, so we used the Profilometer Tenco Alpha Step 200 within the Maryland Nanocenter because of its ease of use. Profilometry is a technique whereby a tip is dropped onto a substrate and dragged across the surface, detecting changes in its height as it goes across. The technique is somewhat crude, but simple to perform. The information from profilometry let us know what kind of thicknesses we could expect using our different deposition methods, and it also gave us qualitative information about roughness which we analyzed further using atomic force microscopy (AFM). The thickness of each layer was also needed to accurately use the equations in our modelling. To prepare our samples for profilometry, we deposited the polymers onto glass slides with tape protecting part of the glass from the film. This gave us an interface to compare film thickness to. We took several profilometry scans for each film to ascertain a consistent thickness number. For all of the spin coated polymers, the thickness was about 70 nm. For drop-cast PANI, the thickness
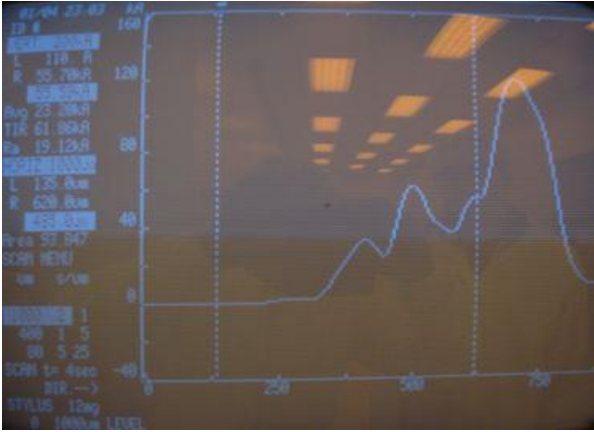
was about 4 μm. For the sputtered Mg$_4$Ni/Pt, the whole layer was about 200 nm. Several images we obtained using this instrument are shown in Figures 25, 26, and 27, for PEDOT:PSS, PEI, and PANI layers, respectively.

Figure 24: A profilometer measurement of a spin coated PEDOT:PSS film on glass. The measurement reads a thickness of about 67.5 nm.

Figure 25: A profilometer measurement of a spin coated PEI film on glass. The measurement reads a thickness of about 65 nm.

Figure 26: A profilometer measurement of a drop-cast PANI film on glass. The measurement is very rough, but after conductive several scans, the average thickness was about 4 μm.

Using equation (8), we were able to determine that we needed a ~2 μm thick layer of PANI to make a working device. Although profilometry shows that the surface of PANI tends to be rough, we knew that spin coating 30 layers of 70 nm PANI films would take too long as compared to drop casting the polymer.

Atomic Force Microscopy

An important consideration in accurately modelling the optical properties of our device was surface roughness for each of our thin film layers. A surface which oscillates with wavelength comparable to the wavelength of light hitting the surface may cause the light to scatter in unanticipated directions, limiting the transmittance of a working device. In order to gauge how rough each of our layers was, we decided to perform atomic force microscopy (AFM).

Atomic force microscopy involves piezoelectrically driving a cantilever with a sharp tip across the surface of a material while monitoring and correcting for changes in the interatomic attractive forces—such as Van der Waals forces—which arise as the cantilever tip approaches the surface only a few atomic spaces away. There are three main operating modes for an AFM: contact mode, noncontact mode, and tapping mode. Contact mode involves rastering the cantilever tip at a constant distance from the surface in order to maintain a constant force, and the associated changes in height the tip makes can be

recorded to map topography of material surfaces. Noncontact mode involves driving the cantilever close to resonant frequency above a surface. Changes in interatomic forces in this mode cause shifts within resonant frequency which can be counteracted and monitored by adjusting the driving voltage, also allowing for a map of the surface. Tapping mode is a special variant of noncontact mode in which the driving amplitude is large enough that the tip repeatedly contacts the surface without dragging along it.[16]

Our group used an AFM in atmospheric conditions available to us within the Modern Engineering Materials Instructional Laboratory (MEMIL) within the Kim building. This instrument detects deflection in the cantilever optically, by monitoring the deflection of a laser reflecting off the back of the cantilever as it moves, which is common for many commercial AFMs.[16] Originally, we intended to operate the AFM in noncontact mode to minimize the risk of dragging polymeric molecules across the surface of our films, which is likely to happen in contact mode, but Dr. Aldo Ponce, who supervised us on the instrument, had not calibrated the machine for an accurate topography measurement in noncontact mode. Thus, we operated the AFM in contact mode at a constant force of 15-25.6 nN, which we altered depending on measurement artifacts indicating too strong an interaction with our material surfaces.

We used the AFM to map the surfaces of a PEDOT:PSS film deposited by spin-coating, a PANI film deposited by spin-coating, a PANI film deposited by drop-casting, a Mg_4Ni/Pt film deposited by sputtering, and our glass slides. For each material, we took scans 10x10, 20x20, and/or 100 x 100 μm in area in three separate locations. We took the data from each location, and used a software package called Gwyddion which allows analysis of such data. Using the software, we were able to take several line scans for each measurement and obtain root-mean-square (RMS) roughness values. For each measurement, we took 10 line scans, and averaged the values of the RMS roughness for each material.
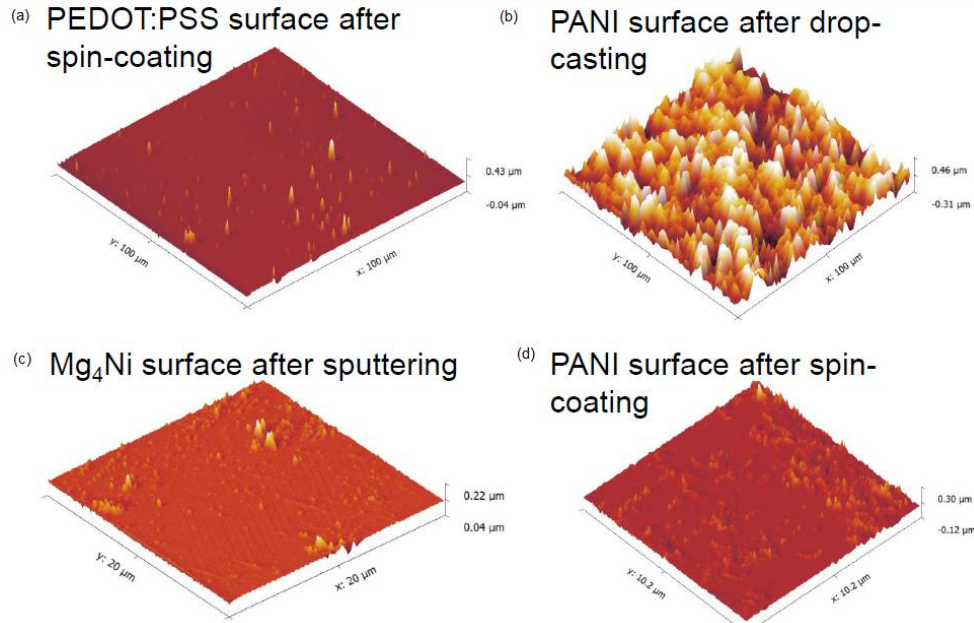
Figure 27 These are 3D topographical maps obtained by performing AFM on (a) spin-coated PEDOT:PSS, (b) drop-cast PANI, (c) Mg_4Ni/Pt, and (d) spin-coated PANI. The maps were generated by feeding the AFM raw data into a software package called Gwyddion. This software allows one to perform line scans across the image in order to obtain values of roughness. We performed 3 measurements per material, and 10 line scans per measurement to estimate the RMS roughness of each material. Just judging by the images, however, it's clear the drop-casting PANI creates a very rough interface.

Table III summarizes the results for the thickness of each of our layers and each layer's RMS roughness, and Figure 27 shows 3D topographical maps characteristic for spin-coated PEDOT:PSS, drop-cast PANI, sputtered Mg_4Ni, and spin-coated PANI. For every layer except the drop-cast PANI, the RMS roughness is between 5-15 nm, a quantity small enough that we believe scattering due to roughness between interfaces can be ignored to simplify optical modelling calculations. However, the RMS roughness for the drop-cast PANI—the method by which we deposited PANI for our actual device—is considerable at 130.16 nm. Despite our decision to drop-cast PANI in order to fabricate a 4 μm layer in a timely fashion, our AFM results clearly indicate spin-coating is the superior method to fabricate as flat a layer as possible.

Material	Thickness	RMS Roughness (nm)
PEDOT:PSS spin-coat	~70 nm	7.59
PEI spin-coat	~70 nm	Equal to PANI
PANI spin-coat	~70 nm	12.36
PANI drop-cast	~4 μm	130.16
Mg4Ni/Pt sputtered	200 nm	4.67
Glass	1.5 mm	5.27

Table III A summary of the results from our profilometry and AFM measurements for each of our thin film materials.
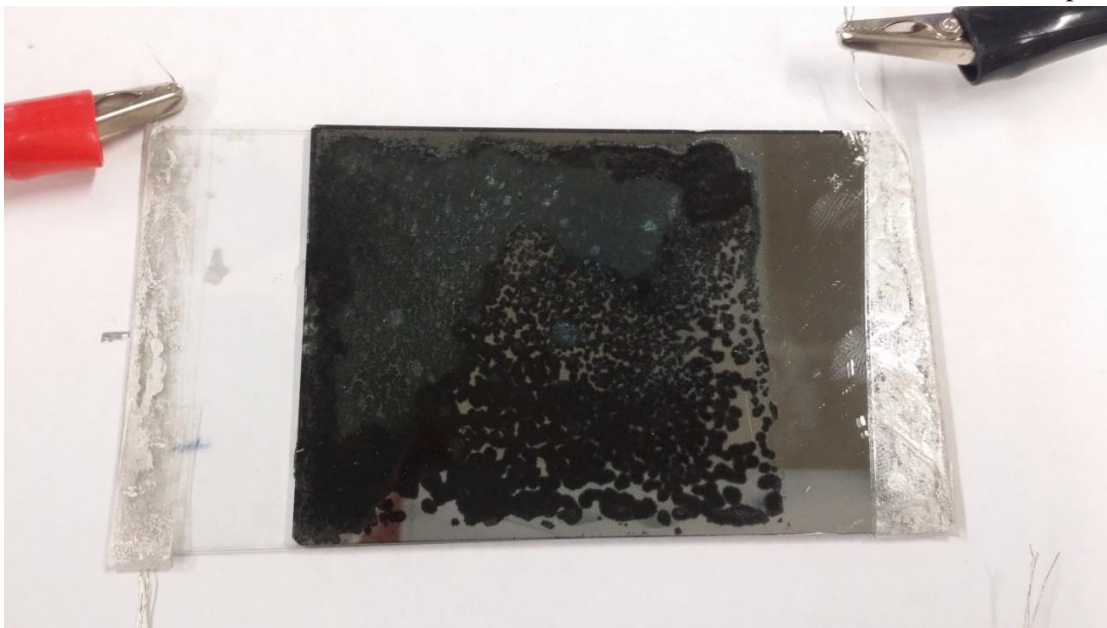
Figure 24 This is a picture taken of the second prototype of our device with electrical connections. One the sides of the glass slides, wires were adhered using silver paste to make contact with the PEDOT:PSS electrodes, and alligator clips connected to a power supply were attached to the wires. When we applied a voltage, however, no current moved through the device. We believe this is a result of unresolved contact issues that arose during fabrication.

Electrical Tests

To test our prototypes, we made contact with our thin films devices by adhering wire connections to the sides of glass slides with silver paste. These wires we clamped with alligator clips connected to a Keithley Model 2200-20V-5A power supply. A set-up of this connection is shown in Figure 24. The supply allowed us to output a voltage and read the current across our device with a resolution of ± 0.1 mA.

Our original idea was to perform qualitative tests using this set-up in order to estimate switching time for our devices. If we could affect an optical change under 5V after a specific amount of time, judged subjectively by our perception of the optical properties, this switching time would give us a good figure of reference to validate or invalidate our electrical predictions.

Unfortunately, our prototype devices suffered from poor contact issues. For our first device, we were able to introduce an optical change in a small area of the sample, shown in comparison to our second device in Figure 25. Under an applied 5V, the current began at about 1.1 mA before slowly dwindling down to 0, or an undetectable amount, over the course of 1143 s, or ~20 min. This current is much less than we anticipated, and the fact that it diminished to 0 over the course of applying the voltage signals to us two things: (1) we have overestimated the hydrogen conductivity of one or more of our layers or (2) we have poor contact in the ultimate device.

We believe poor contact is more likely for several reasons. The first reason is that our second prototype, manufactured by the same processes, did not have any current run through it for applied voltages 5, 10, 15, and 20V. The second reason is that there appeared to be peeling of the conductive PEDOT:PSS layer on the second prototype we put together, which might attest to problems we did not
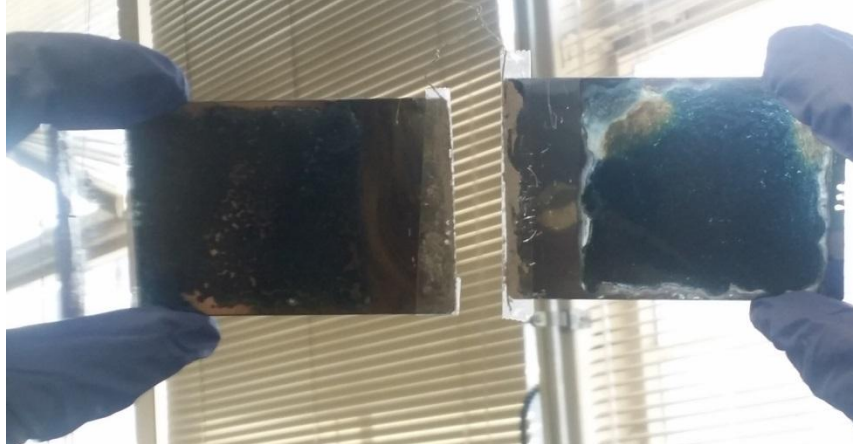
Figure 25 This picture shows a comparison between our first prototype, which we were able to put a voltage through for a short time, and our second prototype, which we could not make contact with. A scant transmission of light can be seen around the borders of our first prototype, showing we were able to affect a change in transparency.
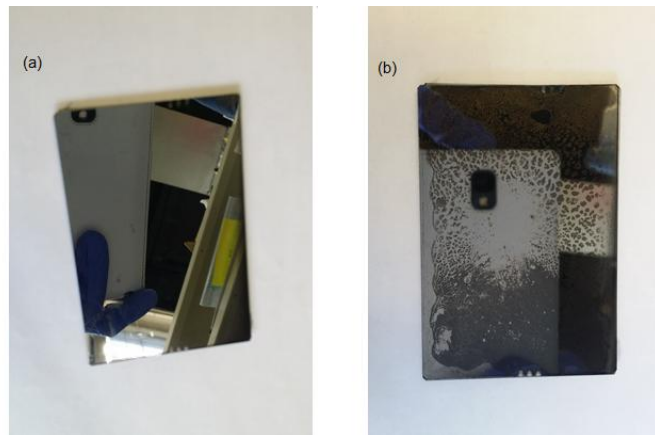

Figure 26 These two pictures show (a) a glass/Mg_4Ni/PEI/PANI/PEDOT/glass device a few seconds after adhering the device and (b) five minutes after. It appears a reaction spontaneously occurs as hydrogen diffuses out of the PANI and into the alloy without any electrical driving force. This we believe is a result of too thin a layer of PEI, and it could also be the reason we have poor electrical contact across the device.

see in putting together both devices. The third reason is that, based on our profilometry and AFM measurements, the thickness of PEI 70nm, was about half the RMS roughness of our drop-cast PANI, 130.16 nm. We believe that this discrepancy could have caused very poor adhesion between the PANI and Mg_4Ni layer, ruining the contact.

One interesting phenomenon we observed right before putting together this report is that, upon adhering the PANI to the Mg_4Ni, there appeared to be a spontaneous reaction between the layers without an applied voltage, causing intermittent spots of Mg_4Ni/Pt to transform to MgH_2/$MgNiH_4$/Pt in irregular fashion. We captured this in a picture shown in Figure 26. This raises a lot of questions about the stability of our layers, which we believe would need further investigation via adjustments of the thickness of the PEI layer by further deposition, or flattening of the PANI layer by spin deposition.
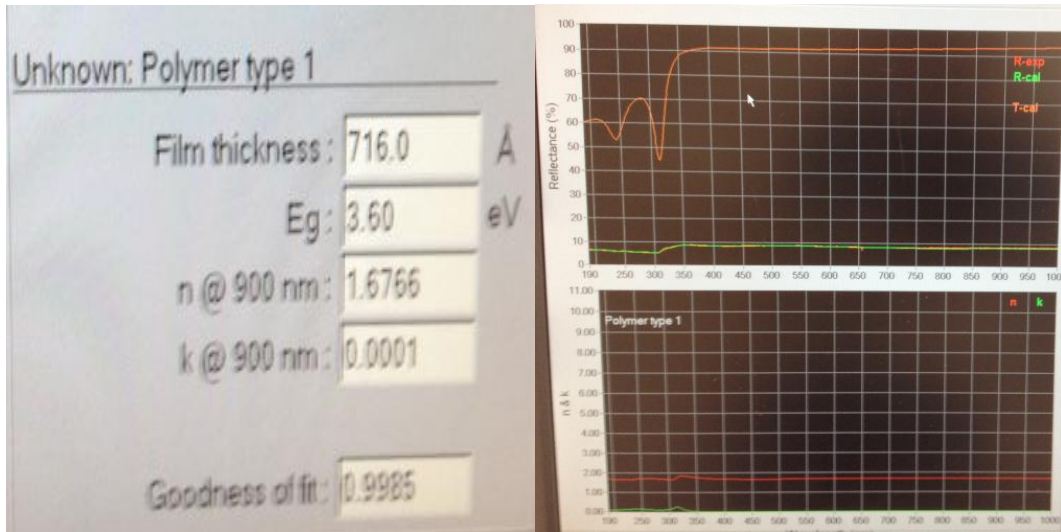
Figure 27 The results of an N&K Spectrophotometer measurement of PEDOT:PSS on glass. By using the default settings of a polymer on a glass substrate for the machine, we were able to obtain a reasonable measurement, yielding 1.68 + 0.0001 as the refractive index for PEDOT:PSS at 900 nm.
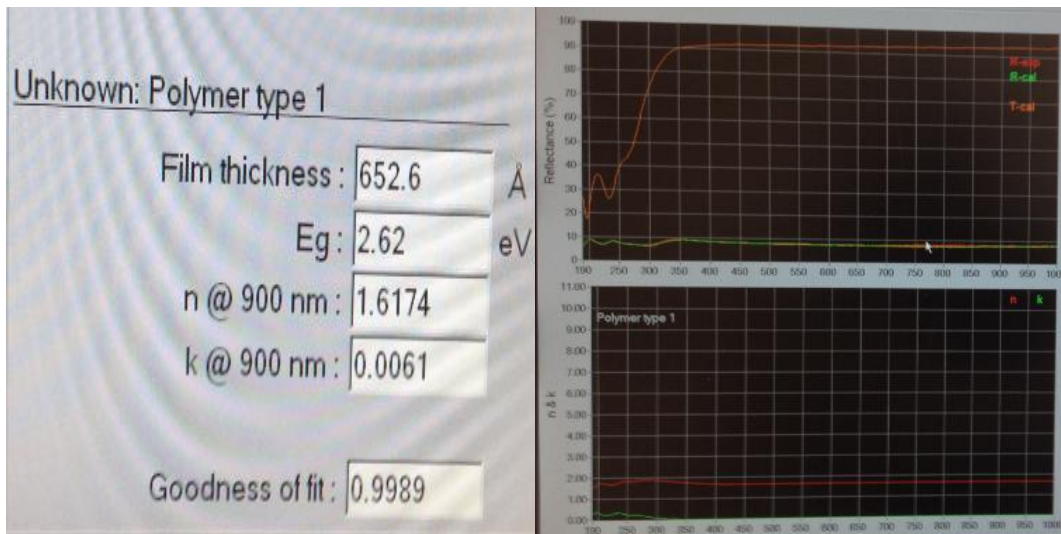

Figure 28 The results of an N&K Spectrophotometer measurement of PEI on glass. We were also able to obtain a reasonable measurement using default settings of the instrument, yielding a refractive index of 1.62 + 0.0061i at 900 nm for PEI.

N&K Spectrophotometry

After we successfully deposited PANI, PEDOT:PSS, and PEI on our glass slides, we tried to characterize the refractive index and transmittance of each layer. We searched around the instruments

available to us around the university which could measure the refractive index. Among the machines, we decided to use the N&K spectrophotometer that in the Maryland Nanocenter because the machine sounded simple to use and could accommodate the size of our samples.

The machine emits a spectrum of light from 100-1000 nm in wavelength across the surface of a thin film sample. Reflected and transmitted light is caught by a collector of the machine, and the software package for the instrument can calculate indices of refraction along specific wavelengths. By using the N&K spectrophotometer, we figured out the index of refraction of PEDOT:PSS layer is 1.68 at 900 nm and the index of refraction for PEI is 1.62 at 900 nm. We think this result is reasonable because the machine also detects the film thickness and reported value similar to that of the profilometer. Images we capture of these measurements are shown in Figures 27 and 28.

However, when we tried to measure the refractive index of PANI, the N&K spectrophotometer did not yield any useful data. We believe this is due to that fact that the PANI is much more absorptive and rougher than the PEDOT:PSS and PEI films. The N&K spectrophotometer might not be able to hand such a material. Furthermore, using the machine requires a good amount of expertise to set up measurements. The software package was obtuse and required specific inputs which the lab technician did not understand nor could he help us with. Due to this unexpected situation, we found that we could not take accurate measurements using the N&K spectrometer within the time constraints of the semester for PANI, Mg_4Ni/Pt, or the final device. . In the future, we would have to gain a much better understanding of the instrument, or resort to a different measurement method.

Energy-dispersive X-ray Spectroscopy

Energy-dispersive X-ray Spectroscopy (EDS) is a compositional analysis technique which detects characteristic elemental X-rays of a sample after being bombarded with standardized Cu X-rays. The amount of each X-ray detected for each element allows one to determine the relative amount of each element present.

We wished to perform EDS on our Mg_4Ni/Pt layer after sputtering in order to assess the efficacy of our sputtering conditions. Unfortunately, by the time we had a sample ready for analysis, the machine we were scheduled to use went down for repairs, and it was not possible to use the instrument before presenting our results. The information we would have obtained could have been very helpful in determining what might have gone wrong in the electrical testing of our device. Without it, we have assumed we obtained the right composition, but the test still needs to be done to confirm this.

Conclusions and Future Work

Our group acknowledges there is much more characterization work to be done in order to validate our models and make them more accurate. In order to properly model the optical properties of our device, we need to do full assays on the dielectric constant as a function of frequency for each material. In the case of Mg_4Ni/Pt and PANI, measurements would have to be done between the hydrogenated and dehydrogenated states. In addition to N&K spectrophotometry, it might be more prudent to instead make a capacitor out of each layer in order to obtain the optical properties we need. This investigation would require an approach to synthesis quite different than the one we took this semester, but it is necessary in order to fully understand the materials we chose.

Afterwards, we would have followed a procedure described by a paper by Johnson and Christy on Optical Constants of Noble Metals, which was published in 1972, to better our optical modelling.[17] Because light is transmitted from the sun in all directions, we would have liked to apply Fresnel's equations to our model that also depended on the angle of incidence, to gain an improved modeling of our optical properties. We would have also liked to apply complex valued functions as detailed in Sernelius's work on Optical Response of Thin Films.[15] We would then be able to model a more correct dependence of reflection from a metallic surface, and refraction in a conducting medium, which would help us predict multiple reflections in our optical modeling. Lastly, we would have liked to model the electrochromic effect of our device, as described by Park, Lee and Herman in a paper on multiple reflection effects in reflective measurements of electro-optic coefficients of poled polymers in multilayer structures, which treats multiple scattering effects.[18]

In addition, understanding the mechanisms and kinetics of hydrogen diffusion into and out of Mg_4Ni/Pt and PANI are necessary to fully develop the electrical model we proposed. The σ_i in our electrical equations is an odd conductivity specific to H^+, but our electrical model does not yield insight into the physical meaning or origin of this quantity. In order to make the calculation of the quantity less empirical, we would need to develop a method to measure the flux of hydrogen in and out the materials as a function of voltage. One way of doing so might be to submerse either material in an acidic half-cell where one can control the flow of H^+ with an applied voltage. Measuring the pH as a function of time should allow one to elucidate how easy it to inject hydrogen into and out of Mg_4Ni and PANI.

Though our ultimate prototype did not work as anticipated, we were able to affect a visible change upon the adhesion of PEDOT:PSS/Mg_4Ni/Pt with PEI/PANI/PEDOT:PSS. This indicates to us that the materials selection seems to have worked as intended, but that further design considerations must be taken into account in order to fabricate a switchable mirror which can switch back and forth between transparent and reflecting modes from an applied voltage.

The biggest problem we believe hindered our device performance was the thickness of the PEI layer as compared to the roughness of the PANI layer. The PEI, only 70 nm thick, was half of the 130.16 nm RMS roughness of the 4 μm thick PANI layer. We believe that, because the PEI was so thin, it married the interfaces of PANI and Mg_4Ni/Pt poorly, resulting in poor contact and a spontaneous diffusion path of H^+ from PANI to Mg_4Ni/Pt with no intermediate barrier. Thus, we created a device which spontaneously converted portions of Mg_4Ni/Pt to MgH_2/$MgNiH_4$, and which also did not respond well to an applied voltage due to uneven contact and charge distribution.

Another problem we encountered was fabricating layers of Mg_4Ni/Pt which were too thick, increasing the thickness requirements of the PANI as well as the projected switching time for our device. We were not sure of the deposition rate when we initially sputtered our Mg_4Ni layer, but the results from our sputtering session allowed us to determine a sputtering rate of 0.28 nm/s. In future sessions, it is reasonable that we could tailor the Mg_4Ni layer to the exact thickness we would like.

As a result of all that we learned from our processing and characterization for each separate layer, we believe we could make a much more successful device for future work. We know now that spin-coating yields films with RMS roughness on the order of 8-15 nm, a roughness small enough that we can idealize flat interfaces for optical modelling. Furthermore, flat interfaces between the Mg_4Ni and PANI would make them easier to adhere together with the PEI. In anticipation of creating a bigger diffusion barrier so that the H^+ from the PANI does not spontaneously diffuse into the Mg_4Ni, we might ever want to drop-cast the PEI before sandwiching all the layers together. For future work, we propose making a device as follows:

1. Spin-coat 70 nm of PEDOT:PSS onto two glass substrates.
2. On one PEDOT:PSS/glass substrate, sputter ~40nm of Mg_4Ni onto PEDOT:PSS in an AJA sputtering unit with $2*10^{-6}$ Torr base pressure, 7.5 mTorr working pressure, 110 mm target-to-substrate distance, 200 W Mg, 105 W Ni, at a rate of 0.28 nm/s.
3. Spin-coat 6 70 nm layers of PANI onto the other PEDOT:PSS/glass substrate.
4. Drop-cast PEI onto PANI/PEDOT:PSS/glass.
5. Adhere the layered halves.

These processing steps we believe would lead to a more successful device, and, if not, they might give more insights into the mechanisms of hydrogen diffusion going on between the separate layers.

However, even if we were to fabricate a working device, the question arises as to whether or not such a process lends itself to commercialization of a window 2 x 3 m^2 in size, an area considered a benchmark figure for smart window production.[1] We believe that spin-coating flat polymer layers 70-400 nm in size would be unfeasible for such an endeavor, and sputtering Mg_4Ni/Pt onto a sheet of glass that large would require a sputtering chamber far too large to be reasonable. However, in comparison to the expense of creating windows that size covered with ITO and WO_3, our process is much cheaper.

Acknowledgements

References

1. Baetens R, Jelle BP, and A Gustaven. "Properties, requirements and possibilities of smart windows for dynamic daylight and solar energy control in buildings: A state-of-the-art review." Solar Energy Materials and Solar Cells, vol. 94; pp.87-105. 2010.

2. Tajima K, Hotta H et al. "Electrochromic switchable mirror glass fabricated using adhesive electrolyte layer." Applied Physics Letters, vol. 101. 2012.

3. Kirchmeyer S and K Reuter. "Scientific importance, properties, and growing applications of poly(3,4-ethylenedioxythiophene)." Journal of Materials Chemistry, vol. 15; pp. 2077-88. 2005.

4. Deepa M, Ahmad S, et al. "Electrochromic properties of polyaniline thin film nanostructures derived from solutions of ionic liquid/polyethylene glycol." Electrochimica Acta, vol. 52; pp. 7453-63. 2007.

5. Yoshimura K, Yamada Y and M Okada. ""Optical switching of Mg-rich Mg-Ni thin films." Applied Physics Letters, vol. 81; iss. 25; pp. 4709-11. December 16, 2002.

6. Lubianez R, North America Sales Manager of Hereaus Precious Metals (personal communication, February 19, 2014).

7. Li D, Huang J, and RB Kaner. "Polyaniline nanofibers: A Unique Polymer Nanostructure for Versatile Applications." Accounts of Chemical Reserach, vol. 42; iss. 1; pp. 135-45. 2009.

8. Richardson TJ, Slack JL, et al."Switchable mirrors based on nickel-magnesium films." Applied Physics Letters, vol. 78; iss. 20, pp. 3047-9. May 14, 2001.

9. Rakić AD, Djurišic AB, Elazar JM, and ML Majewski. "Optical properties of metallic films for vertical-cavity optoelectronic devices." *Appl. Opt.,* vol. **37**; pp. 5271-5283. 1998.

10. Callister, WD, and DG Rethwisch. *Fundamentals of materials science and engineering: an integrated approach.* 3rd ed. Hoboken, NJ: John Wiley & Sons, 2008. Print.

11. Liu Y, and DR Schmitt. "The Transition Between the Scale Domains of Ray and Effective Medium Theory and Anisotropy: Numerical Models." *Pure and Applied Geophysics* 163.7 (2006): 1327-1349. Print.

12. Ricoy MA and JL Volakis. "Derivation of generalized transition/boundary conditions for planar multiple-layer structures." *Radio Science* 25.4 (1990): 391-405. Print.

13. Mo Dang, et al. "Ellipsometric Spectra and Refractive Index of Polyaniline." Chinese Phys. Lett. November 3, 1992. Vol. 10, No. 6. 374. PACS: 78.65.Hc, 78. 40. –q, 07. 60. Fs, 78. 20. Ci

14. M. Rubin. "Optical properties of soda lime silica glasses." Solar Energy Materials (1985). Vol. 12, Pg. 275-288

15. Bo E. Sernelius. "Optical Response – Thin Films." From Dr. Phaneuf. Not found by any other name online.

16. Phaneuf RJ. "Atomic Force Microscopy." Lecture notes prepared for course ENMA441. Downloaded from Canvas on May 13, 2014.

17. Johnson PB and Christy RW. "Optical Constant of Noble Metals." *Physical Review B* 6.12 (1972).:4370-4379. Print.

18. Park DH, Lee CH, and WN Herman. "Analysis of multiple reflection effects in reflective measurements of electro-optic coefficients of poled polymers in multilayer structures." *Optics Express* 14.19 (2006): 8866. Print.